PHILOSOPHICAL TRANSACTIONS OF THE ROYAL SOCIETY A MATHEMATICAL, PHYSICAL & ENGINEERING SCIENCES

The Deep Impurity $\rightarrow $ Conduction Band Charge Transfer Transition in ZnSe:Co

D. J. Robbins, P. J. Dean, C. L. West and W. Hayes

Phil. Trans. R. Soc. Lond. A 1982 **304**, 499-531
doi: 10.1098/rsta.1982.0019

Phil. Trans. R. Soc. Lond. A **304**, 499–531 (1982) [499]
Printed in Great Britain

THE DEEP IMPURITY → CONDUCTION BAND CHARGE TRANSFER TRANSITION IN ZnSe:Co

BY D. J. ROBBINS†‡, P. J. DEAN†, C. L. WEST§‖ AND W. HAYES§

† *Royal Signals and Radar Establishment, St Andrews Road, Great Malvern, Worcestershire WR14 3PS, U.K.*

§ *Clarendon Laboratory, Parks Road, Oxford OX1 3PU, U.K.*

(*Communicated by E. R. Pike, F.R.S. – Received 22 June 1981*)

CONTENTS

Novel absorption and luminescence features observed in ZnSe:Co were described briefly in a recent paper. The associated transitions involve three high energy excited states, L, M and N, of Co^{2+}_{Zn}. This is established from the appearance of these transitions in the excitation spectra of the $^4T_2 \rightarrow {}^4A_2$ infrared luminescence of Co^{2+}_{Zn} and the observation of luminescence from the lowest excited state L to four different spin quartet states of Co^{2+} whose energy separations are accurately known from infrared absorption. The present paper contains a much more complete account of the experi-

‡ Present address: IBM Watson Research Center, Yorktown Heights, New York 10598, U.S.A.
‖ Present address: Royal Signals and Radar Establishment, St Andrews Road, Malvern, Worcestershire WR14 3PS, U.K.

mental properties of these new transitions, including a detailed study of the magneto-optical properties and behaviour under uniaxial stress of transition L and its satellites. Among three possible models for the new states, two are discarded, particularly in view of the weak phonon coupling and the symmetric positive form of the L, M and N absorption lines. The remaining model is closely associated with the impurity → conduction band charge transfer process since the excited states are described with two weakly interacting parts, the Co^{3+} impurity core and a relatively weakly bound electron in three different symmetric excited states. The symmetry and g-value of excited state L are readily described by a Hamiltonian containing spin–orbit and exchange interaction terms. However, the properties of the lower satellite L′ (2.363 eV) indicate a vibronic character which requires a dynamic Jahn–Teller interaction term. The parameters of the model required by experiment appear reasonable.

1. Introduction

Cobalt doping of ZnSe produces mainly the $Co^{2+}_{Zn}(d^7)$ impurity charge state (Ham *et al.* 1960). The d–d ligand field spectrum of this impurity has been studied by many workers, and is now well known (Baranowski *et al.* 1967; Wray & Allen 1971; Radlinksi 1977, 1978; Uba & Baranowski 1978). The major features in the absorption spectrum are three spin-allowed transitions originating from the $^4A_2(F)$ ground state, giving rise to zero-phonon lines (z.p.l.) near 0.409 eV ($^4T_2(F)$), 0.690 eV ($^4T_1(F)$) and 1.630 eV ($^4T_1(P)$). In addition the $^4T_2(F) \rightarrow {}^4A_2(F)$ transition produces a strong infrared (i.r.) luminescence band at low temperature. Radlinski (1979) proposed from photoconductivity studies that the $^4A_2(F)$ ground state of Co^{2+}_{Zn} is situated *ca.* 0.69 eV below the conduction band (c.b.) of ZnSe. However, more recent photocapacitance measurements clearly show that the ground state in the reaction $Co^{2+}(d^7) \rightarrow Co^{3+}(d^6) + e_{c.b.}$ lies much closer to the valence band (v.b.) (Noras *et al.* 1980).

In an earlier paper (Robbins *et al.* 1980; hereafter referred to as I) three sharp and relatively weak absorption features in the range 2.36–2.60 eV, near the band-gap of Co-diffused ZnSe, were reported for the first time. Four weak luminescence transitions were observed to originate from the lowest energy of these excited states, terminating on the four spin-quartet states of the $Co^{2+}_{Zn}(d^7)$ impurity centre. This clearly suggested that the three states with z.p.ls at 2.361, 2.432 and 2.546 eV in absorption (here labelled L, M, N respectively) are high energy excited states of the Co^{2+}_{Zn} impurity, a conclusion supported by the observation of the lines L, M and N as strong positive features in the photoluminescence excitation (p.l.e.) spectrum of the Co^{2+}_{Zn} internal i.r. luminescence at 0.409 eV.

The assignment of these higher excited states was not clearly established in I, and three possibilities were discussed:

(i) A charge-transfer (c.t.) state in which an electron is excited from the v.b. *into* an unfilled d-orbital of the Co^{2+}_{Zn} impurity, the resulting hole remaining bound in the coulomb field of the impurity core which is now negatively charged with respect to the lattice. Examples of such c.t. states are known for Ni^{2+}_{Zn} in ZnSe (Bishop *et al.* 1980; Noras & Allen 1980) and Cu^{2+}_{Zn} in ZnO (Dingle 1969; Dean *et al.* 1981*a*; Robbins *et al* 1981).

(ii) An atomic-like (ligand field) spin-doublet excited state of the $3d^7$ configuration of Co^{2+}_{Zn}. A number of doublet states are predicted in this visible spectral region, although experimental evidence for observation of such transitions in absorption is sparse, as might be expected from the influence of the spin selection rule (Wray & Allen 1971; Weakliem 1962; Uba & Baranowski 1978; Weber *et al.* 1980).

(iii) A c.t. state in which an electron is excited *from* a d-orbital of the $Co^{2+}_{Zn}(d^7)$ impurity core into a localized orbital split off from some c.b. minimum (probably Γ) under the influence of the Co impurity potential. The electron would remain bound to the impurity by a combination of central cell forces and the coulomb field of the residual impurity core, which is now positively charged with respect to the lattice. There is no previously established example of such a transition for a transition metal (t.m.) in a semiconductor.

The first of these possible assignments was dismissed in I as being inconsistent with the weak phonon coupling observed for the absorption bands between 2.36 and 2.60 eV. V.b. → impurity c.t. transitions of the kind proposed in (i) are typically strongly phonon coupled, since they involve electron excitation from bonding to antibonding levels in the crystal. This produces a significant weakening of the local bonding in the vicinity of the impurity when the v.b. hole is tightly bound. Electron–hole recombination involving even the shallowest effective-mass (e.m.)-like acceptor in ZnSe ($E_A \approx 85$ meV) (Kosai *et al.* 1979) gives rise to considerably stronger phonon coupling than is observed in these transitions. Arguments based on the observed line-shape of the absorption bands, to be presented later in § 4 of this paper, can similarly be used to discount assignment (ii) to spin-doublet states of the $Co^{2+}_{Zn}(d^7)$ configuration. This therefore leaves (iii), an impurity → c.b. excitation of the c.t. type, as the only assignment that appears consistent with all the experimental observations. To test this hypothesis we have made uniaxial stress and Zeeman measurements mainly on the lowest energy absorption band, since this shows two lines at 2.361 eV (z.p.l.) and 2.363 eV which are sufficiently sharp to allow detailed spectroscopic analysis. As will become clear, these data can be used to provide strong support for assignment (iii) above.

This result is of particular interest for two reasons. First, the identification of such transitions determines the position of the impurity ground state level in relation to the crystal bands, to within the uncertainty of the binding energy of the excited electron. We can estimate this binding energy from the threshold of a broad component with low energy threshold near 2.55 eV, which most probably arises from the photoionization transition. From the combination of absorption and associated luminescence it is possible to deduce both the chemical identity and the energy in the band-gap of the Co^{2+}_{Zn} impurity. Secondly, the excited state of the transition

$$Co^{2+}(d^7) \rightarrow [Co^{3+}(d^6)]\,.\,e_b \qquad (1)$$

can be considered to consist of two relatively weakly coupled parts: (*a*) the residual $[Co^{3+}(d^6)]$ core, which gives rise to a number of different electronic states split by the ligand field; (*b*) the bound electron e_b moving in an orbit derived largely from the c.b. levels of the host crystal. Any theoretical analysis of such an excited state therefore involves elements of both ligand field theory, familiar from internal d–d excitations of t.m. impurities, and of the hydrogenic models widely used to discuss shallower impurity levels in solid-state physics theory. It will be shown that the fine structure in the 2.361 eV absorption band can indeed be accounted for in terms of a spin-determined interaction between the loosely bound electron and the spin–orbit components of the $[Co^{3+}(d^6)]$ core.

The outline of this paper is as follows. The next section describes the experimental techniques, and the results are reported and discussed in § 3. In § 4 the possible assignments are discussed, and it is shown that only assignment (iii) above appears qualitatively consistent with all the experimental observations. In addition § 4 includes a brief discussion of terminology, since it has been pointed out that use of the term 'charge transfer transition' in the solid state requires careful

definition if ambiguity is to be avoided (Allen 1980). In § 5 a simple model is developed for the excited state of the impurity → c.b. c.t. transition described by equation (1). The model involves four disposable parameters, a spin–orbit energy, a spin–spin interaction energy, a phonon energy and a Jahn–Teller coupling energy. It will be shown that with physically reasonable values for these parameters the model is able to predict the symmetries and give a good quantitative fit to the isotropic Zeeman splittings of the two sharp lines at 2.361 and 2.363 eV. In addition it offers an explanation for the strongly anisotropic stress splittings, and for the additional low energy fine structure observed in the absorption band with origin at 2.361 eV.

2. Experimental

Many of the crystals used in these experiments were fine-grain polycrystalline plates grown at A.W.R.E. by chemical vapour deposition. Some were single crystals grown at Durham University by vapour transport. Doping with Co was achieved by evaporating a layer of the metal onto a cleaned sample surface, followed by 24–48 h in-diffusion at 950–1000 °C in an evacuated quartz ampoule in the presence of excess Se.

Cathodoluminescence spectra were obtained with the samples on a cold finger of a continuous flow He cryostat mounted in a 40 keV demountable electron beam system. Spectra were recorded with a 0.6 m $f/7$ monochromator, with the use of a photomultiplier or Ge diode detector cooled to 77 K. Photoluminescence spectra were recorded by using ultraviolet (u.v.) or blue–green light from a Kr laser, blue light from a He–Cd laser or blue light from a jet-stream dye laser with Stilbene 3 dye. In this case, the spectra were recorded on a 2 m $f/17$ spectrograph fitted with a scanning photomultiplier detector under calculator control. A magnetic field of up to 3.5 T was available in the Voigt configuration. P.l.e. spectra were recorded for the *ca.* 0.4 eV i.r. luminescence detected with a PbS photoconductive detector cooled to 200 K and filtered against the *ca.* 0.48 eV d–d luminescence of Ni^{2+}. Coumarin 30 dye was used in the dye laser. Optical transmission spectra were recorded with a W–I_2 light source. The crystals were cooled by direct immersion in liquid He. Some Zeeman measurements of optical transmission were made in the Faraday configuration with a *ca.* 10 T large-bore superconducting magnet, with the crystals again immersed in liquid He. Wider-range p.l.e. spectra were made with a W–I_2 lamp and 1 m $f/7$ monochromator light source, with the crystal cooled on the cold finger of a continuous flow He cryostat. Further Zeeman and the uniaxial stress measurements were made at the Clarendon Laboratory, Oxford. Magnetic fields of up to 7.6 T could be reached by using a mid-plane transverse access coil. To eliminate the effects of helium boiling in the optical path the magnet was used with only its lower coil immersed in liquid. Uniaxial stress measurements were performed in an exchange gas cryostat, the stress being applied through a stainless steel piston. The required mechanical contact between this piston and the sample was made through indium gaskets (West 1980). The excitation source for these experiments was a 100 W quartz iodide lamp.

3. Results and discussions

(*a*) *Luminescence spectra*

Figure 1*a* shows the absorption spectrum of the Co_{Zn} impurity with origin near 2.361 eV, as measured by Noras (1980). Figure 1*c* shows the inverse luminescence transition first reported in I, but now with energy scale *reversed* so as to fall on the same abscissa as 1*a*. Figure 1*b* is the one-

phonon density-of-states for the ZnSe lattice calculated by Kunc *et al.* (1975). It can be seen that the fine structure in the luminescence transition approximately replicates peaks in the phonon density-of-states but the correspondence with the absorption transition is much less good. In particular there are peaks in the absorption at energies less than about 50 cm^{-1} and at *ca.* 195 cm^{-1} above the origin which do not appear in luminescence and which lie in regions of low density of phonon states in ZnSe.

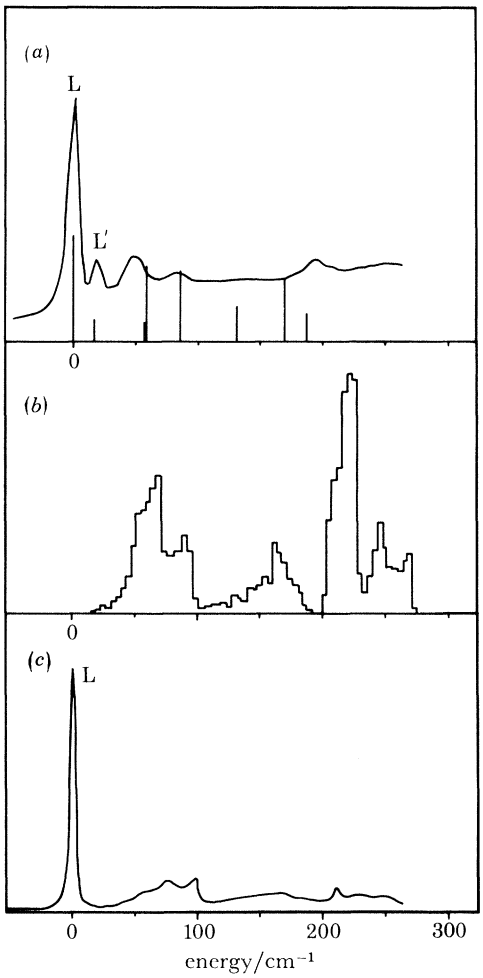

FIGURE 1. Absorption (*a*) (Noras *et al.* 1980) and luminescence (*c*) (Robbins *et al.* 1980) for the impurity → c.b. c.t. transition of Co^{2+}_{Zn} in ZnSe. The luminescence spectrum in (*c*) is plotted on a reversed (negative) energy scale to facilitate comparison with the absorption. The lines in (*a*) are predicted from the model developed in § 5. The z.p.l. at 2.361 eV is denoted L in the text. (*b*) The one-phonon density of states for ZnSe predicted by the deformable-bond approximation (Kunc *et al.* 1975).

In addition to the luminescence band illustrated in figure 1*c*, three weaker transitions originating from the 2.361 eV excited state of the Co_{Zn} impurity can be detected at lower energies. The z.p.ls of these luminescence transitions are listed in table 1 of I, and are there shown to correspond to transitions terminating on the intermediate spin-quartet excited states of the $Co^{2+}_{Zn}(d^7)$ charge state: namely $^4T_2(F)$, $^4T_1(F)$ and $^4T_1(P)$. The luminescence spectra for two of these transitions, L → $^4T_1(F)$ and L → $^4T_2(F)$, are given in figure 2*a* with the regions near the z.p.ls shown on an expanded energy scale in 2*c* and *d*. The lowest energy band L → $^4T_1(P)$ falls very near the end of the responsivity of the Ge detector used to make the i.r. measurement, and

only the two sharp lines shown in figure 2*b* could be detected. However these agree very closely with the predicted z.p.l. energies for the $L \rightarrow {}^4T_1(P)$ luminescence.

It is significant that these luminescence bands originating on the 2.361 eV (L) excited state all terminate on spin-quartet states of the $Co^{2+}_{Zn}(d^7)$ impurity. A feature of the absorption spectrum already noted is that the strong absorption bands all correspond to spin-allowed transitions from the ${}^4A_2(F)$ ground state. This shows clearly that spin is a reasonably good quantum number for the Co_{Zn} impurity in ZnSe, and also suggests that the L excited state itself probably has spin-quartet character in order for it to be detected easily in optical absorption.

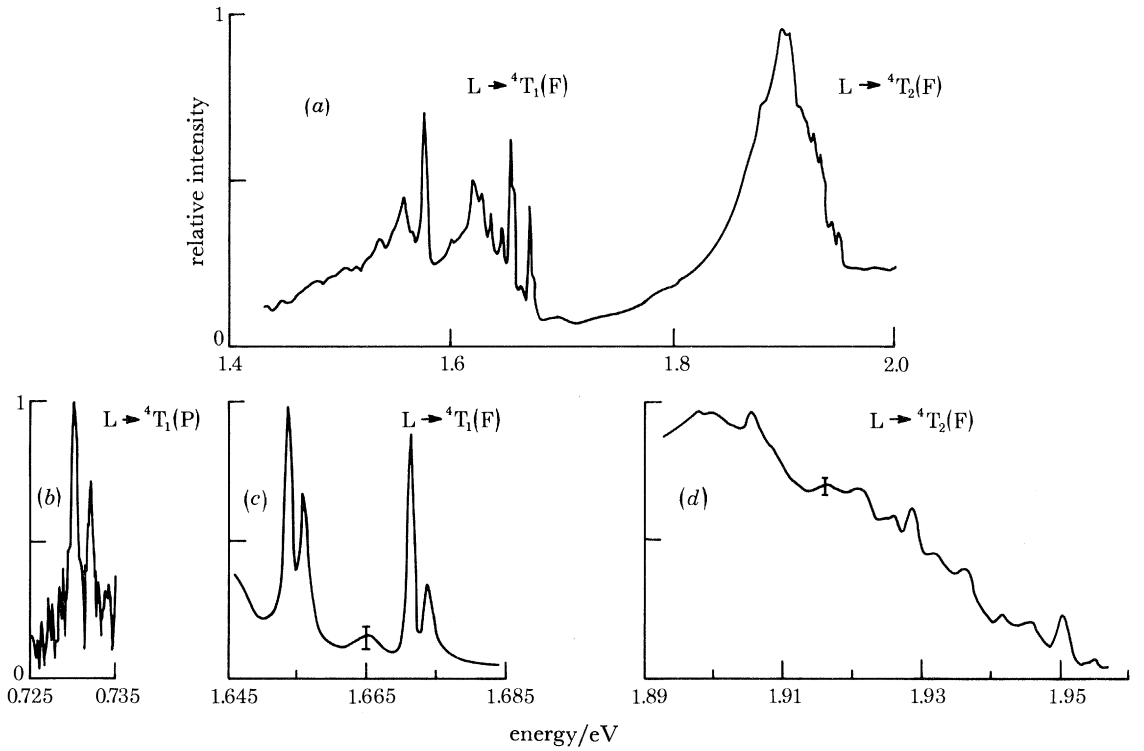

FIGURE 2. (*a*) High-sensitivity cathodoluminescence spectrum of ZnSe:Co excited at 40 keV and detected with a GaAs photomultiplier tube. The two bands are transitions from the c.t. excited state at 2.361 eV (L) to intermediate spin-quartet ligand field states of the $Co^{2+}_{Zn}(d^7)$ impurity. (*c*), (*d*) The origins of these two bands on an expanded energy scale. (*b*) Spectrum was measured by using a Ge detector and shows sharp lines at the origin of a third transition from the L excited state to the highest energy ligand field spin-quartet state of $Co^{2+}_{Zn}(d^7)$. The detector has rapidly decreasing responsivity in this region.

(*b*) *Dye-laser p.l.e. spectra*

The p.l.e. spectrum in the range 2.25–2.85 eV for the Co^{2+}_{Zn} ${}^4T_2(F) \rightarrow {}^4A_2(F)$ i.r. luminescence was reported in I, measured with lamp and monochromator. Although this spectrum indicated the relative intensities of the various excitation features in this region, the signal:noise ratio was only just sufficient to resolve the weaker lines. This p.l.e. spectrum of the i.r. luminescence has therefore been measured by using Coumarin 30 dye laser excitation to confirm the important features reported in I. The higher power available from the dye laser also allows the p.l.e. spectrum of the high energy 2.361 eV luminescence band to be investigated.

Figures 3*a–c* are transmission spectra for Co-doped polycrystalline ZnSe, showing the z.p.ls for the three near-gap absorption bands at 2.361 (L), 2.432 (M) and 2.546 eV (N). Figures 3*d* and *e* show the dye-laser p.l.e. spectra in the region of the first two of these z.p.ls, with a filter

which allowed only the 0.409 eV $Co^{2+}_{Zn}(d^7)$ i.r. luminescence to reach the PbS detector. The 2.361 eV and 2.432 eV z.p.ls appear as strong positive peaks in the p.l.e. spectra, confirming the result reported in I. The tuning range of the Coumarin 30 dye was insufficient to reach the third z.p.l. at 2.546 eV. Figure 3*f* shows the corresponding p.l.e. spectrum near 2.361 eV when all luminescence with wavelength more than 2 μm is allowed to reach the detector. In this case the detected signal is dominated by 0.5 eV $^3T_2(F) \rightarrow {}^3T_1(F)$ luminescence from inadvertent Ni^{2+}_{Zn} impurity in the crystal, which is strongly excited in this spectral region (Bishop *et al.* 1980). The $^4A_2(F) \rightarrow L$ absorption of Co_{Zn} competes with the Ni_{Zn} excitation process, producing a strong negative dip in the p.l.e. spectrum. Figure 3*g* shows the p.l.e. spectrum near 2.432 eV when a photomultiplier is used to detect the visible $L \rightarrow {}^4A_2(F)$ Co_{Zn} luminescence at 2.361 eV. A positive peak is again observed, showing that the 2.432 eV (M) Co_{Zn} excited state is able to relax to the L (2.361 eV) state which can then emit. Lifetime broadening resulting from this relaxation is probably the cause of the increased width of the M and N lines compared with L. As noted in I, the $L \rightarrow {}^4A_2(F)$ luminescence is quite efficiently excited by radiation at the free exciton energy of ZnSe, near 2.802 eV and above. All of these results are consistent with the idea that the absorption bands in figures 3*a–c* represent transitions to high-energy excited states of the Co^{2+}_{Zn} impurity centre.

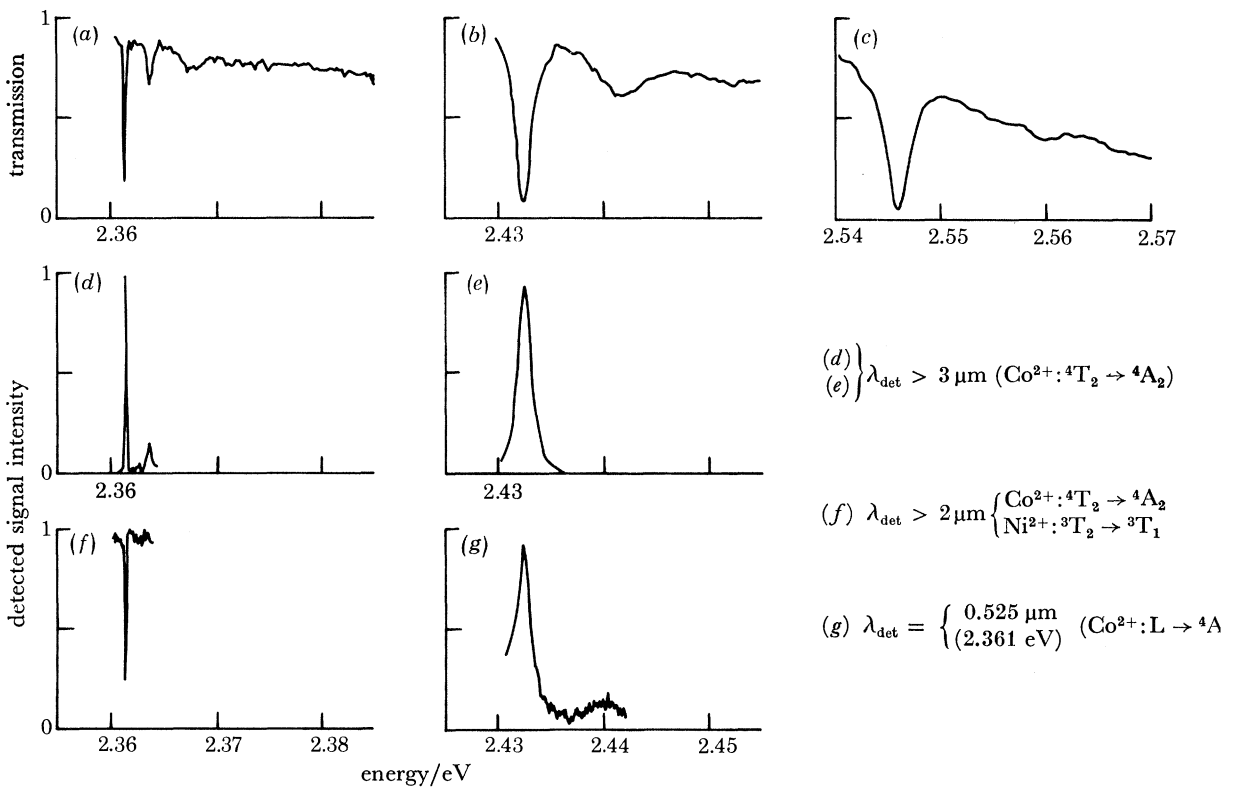

FIGURE 3. (*a*)–(*c*) Transmission spectra of ZnSe:Co. The strong z.p.ls in (*a*)–(*c*) are denoted L, M, N respectively in the text. (*d*), (*e*) P.l.e. spectra of the $Co^{2+}_{Zn}(d^7)$ $^4T_2(F) \rightarrow {}^4A_2(F)$ i.r. luminescence excited by using a dye laser. These spectra confirm earlier results obtained with poorer signal: noise ratio (Robbins *et al.* 1980). (*f*) P.l.e. spectrum for simultaneous detection of i.r. luminescence from a $Ni^{2+}_{Zn}(d^8)$ impurity strongly excited in this spectral region, in addition to the $Co^{2+}_{Zn}(d^7)$ i.r. band. The Co-related L-line absorption competes against the Ni^{2+}_{Zn}-induced luminescence and appears as a strong negative dip. (*g*) P.l.e. spectrum for the 2.361 eV $L \rightarrow {}^4A_2(F)$ luminescence line of Co_{Zn} shown in figure 1*c*.

(c) *Uniaxial stress measurements*

The two low energy absorption lines at 2.361 and 2.363 eV in figure 3*a* are sufficiently sharp (half-widths < 0.5 meV) to produce well resolved splittings under available uniaxial stress and magnetic field perturbations. However, as noted above, the higher energy lines M and N in figures 3*b* and *c* are much broader. Detailed stress and Zeeman measurements have therefore been restricted to the absorption lines at 2.361 and 2.363 eV, designated L and L′ respectively.

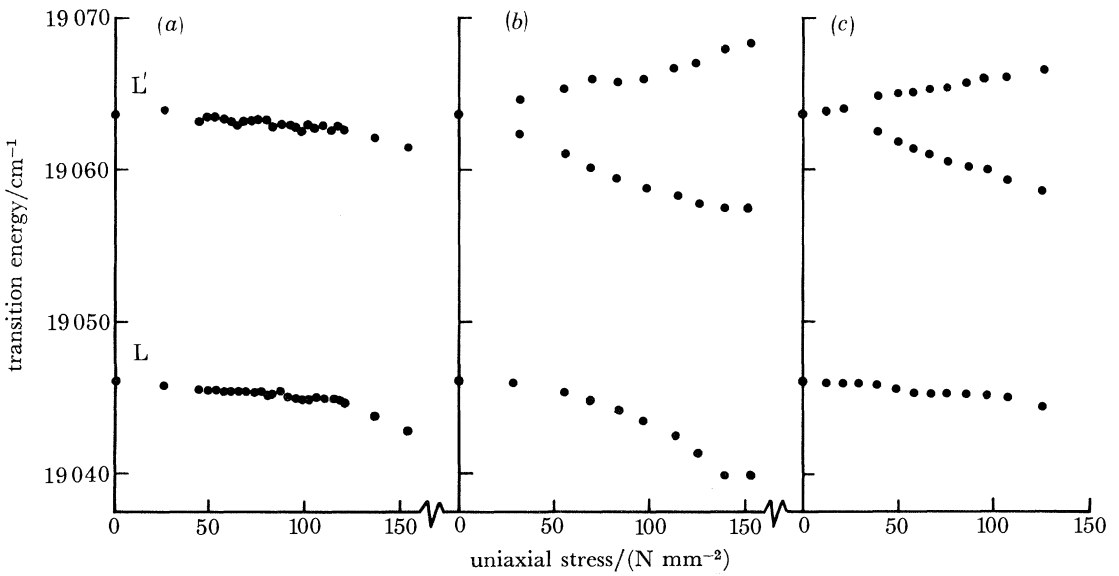

FIGURE 4. Summary of uniaxial stress measurements on the lowest energy components of the c.t. spectra of ZnSe:Co, obtained in transmission. Only these two lines at 2.361 eV (L) and 2.363 eV (L′) are sufficiently sharp to produce well resolved splittings under the experimental conditions. At the higher stresses the crystals show signs of yielding. (*a*) $P \parallel [001]$; (*b*) $P \parallel [111]$; (*c*) $P \parallel [110]$. The stress-induced splitting of the L′ line shows the excited state to have U′ symmetry.

The behaviour of these lines for stress applied along the three principal crystal directions of single-crystal ZnSe:Co is summarized in figure 4. Under stress $P \parallel [001]$ both the L and L′ lines move linearly with increasing stress but do not appear to split. For stress more than 118 N mm^{-2} the crystal tends to yield, producing a quadratic trend. The line L′ splits into two resolved components for stress applied along [111], however. The mean position of these two components follows the isotropic shift observed for the [001] direction. For low stress (less than 69 N mm^{-2}) the main line L shows only the isotropic shift, but under higher stress a second-order mixing with the lower energy component of line L′ becomes evident. A transfer of oscillator strength accompanies this mixing, as can be seen from figure 5.

The ground state of the transitions giving rise to lines L and L′ is the fourfold degenerate U′[^{4}A$_2$(F)]† spin–orbit state of Co^{2+}_{Zn}. Since applied stress does not lift spin-degeneracy in first order, stress-induced splitting of this orbitally non-degenerate ground state can only occur through second-order spin–orbit effects and is therefore expected to be weak. In the comparable case of Co^{2+}_{Ga}(d^7) in GaP the U′[^{4}A$_2$(F)] splitting at the highest stresses applied here was *ca.* 2 cm^{-1}

† We use the group theoretical notation and coupling coefficients given by Griffith (1964). The equivalent (Bethe) notation is: $A_1(\Gamma_1)$; $A_2(\Gamma_2)$; $E(\Gamma_3)$; $T_1(\Gamma_4)$; $T_2(\Gamma_5)$; $E'(\Gamma_6)$; $E''(\Gamma_7)$; $U'(\Gamma_8)$.

(West 1980), which would not be resolved in these measurements. The splitting of line L′ for $P \| [111]$ therefore reflects an excited-state splitting, and this excited state must have U′ symmetry in the T_d double group. The stress pattern can be described in terms of parameters A_α, B_α, C_α, where $\alpha = u, l$ for the upper and lower states and A, B, C describe the response to isotropic, tetragonal and trigonal stresses respectively. The values derived from the experimental data are:

line L, $$(A_u - A_l) = -0.010\,\mathrm{cm^{-1}/(N\,mm^{-2})}; \quad (2)$$

line L′, $$(A_u - A_l) = -0.008\,\mathrm{cm^{-1}/(N\,mm^{-2})}, \quad (3)$$

$$|B_u| < 0.003\,\mathrm{cm^{-1}/(N\,mm^{-2})}, \quad (4)$$

$$C_u = -0.066\,\mathrm{cm^{-1}/(N\,mm^{-2})}. \quad (5)$$

A useful check on the consistency of the analysis is obtained from measurements with stress applied along [110]. From the formulae of Kaplyanskii (1964) the splitting of a U′ state for $P \| [111]$ and $P \| [110]$ should be in the ratio $2C_u/\sqrt{3}:C_u$, in good agreement with the data in figure 4. Kaplyanskii's analysis can also be used to predict the relative intensities of the two

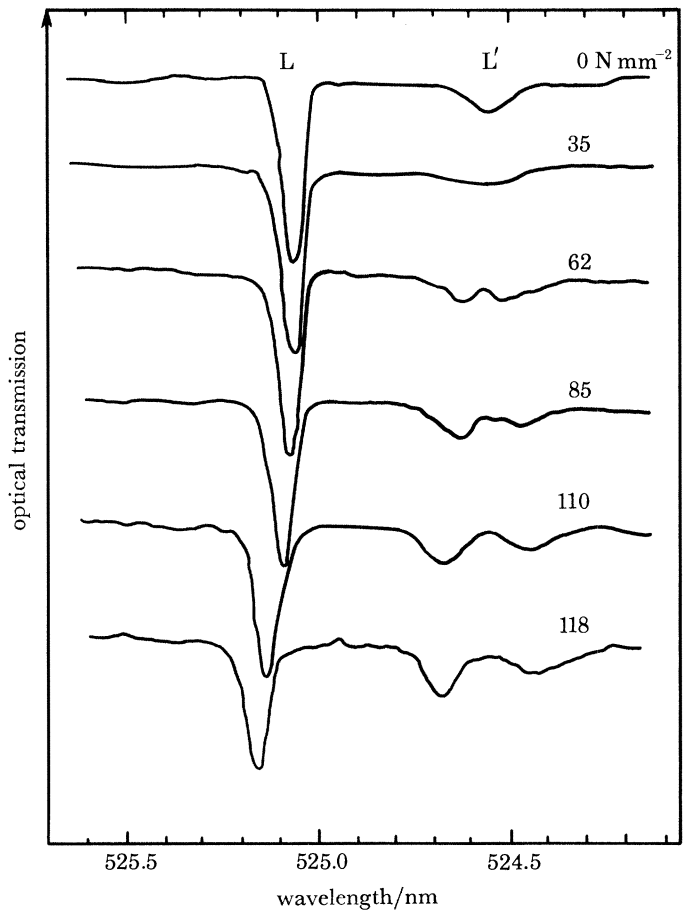

FIGURE 5. Piezo-transmission spectra of the 2.361 eV (L) and 2.363 eV (L′) transitions of ZnSe:Co with increasing stress applied parallel to [111]. The L′ line splits into two resolved components. The lower energy component mixes with the L line at the higher applied stresses, producing a nonlinear splitting and a transfer of oscillator strength.

components of line L′ for polarizations $E \parallel P$ and $E \perp P$. The spectrum in figure 6 was measured for $P \parallel [110]$, with the light vector $\boldsymbol{k} \parallel [001]$. The predicted intensities for a $U'(^4A_2) \rightarrow U'$ transition in this configuration with unresolved ground-state splitting are shown in figure 6, in good agreement with the observed spectrum. Further details of this calculation are given elsewhere (West 1980).

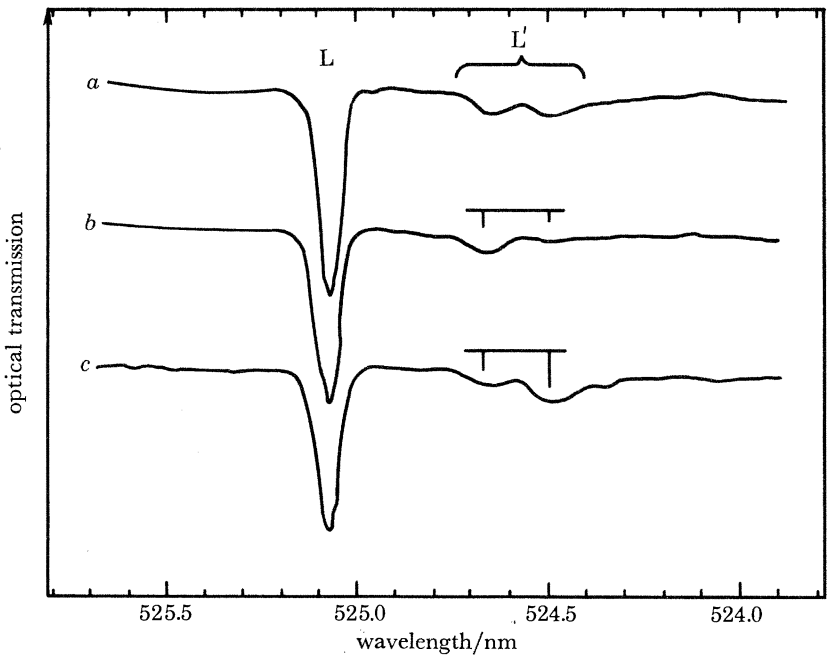

FIGURE 6. Polarized piezo-transmission spectra of the 2.361 eV (L) and 2.363 eV (L′) transitions of ZnSe:Co for stress $P = 95$ N mm^{-2} applied parallel to [110] ($\boldsymbol{k} \parallel [001]$). The lines represent predicted relative intensities for a $U' \rightarrow U'$ transition with unresolved ground-state splitting (see also West 1980): *a*, unpolarized spectrum; *b*, $E \perp P$; *c*, $E \parallel P$.

(*d*) *Zeeman measurements*

The unpolarized splitting of the absorption lines L and L′ for a magnetic field $B = 3.5$ T applied in Voigt configuration along different crystal directions is illustrated in figures 7 (ii)–(iv). Within the resolvable line-widths the Zeeman spectrum is effectively isotropic. The polarizations of the lines for $B \parallel [001]$ are shown in figures 7 (v) and (vi). Line L shows components polarized both $\sigma[E \perp B]$ (labelled *a* and *c*) and $\pi[E \parallel B]$ (labelled *b*), with weaker thermalized components at lower energy. On the other hand, line L′ gives rise to a dominantly π-polarized component (labelled *d*). The temperature dependence of the intensity of these components is indicated in figure 8, where it can be seen that lines *c* and *d* are the strongest features at low temperature (1.6 K). (The strongest line *c* appears in the π-polarized spectra of figures 8 (ii) and (iv) because of slight misalignment of the polarizer). Lines *c* and *d* are therefore 'cold' and originate from the lowest energy $M_S = -\frac{3}{2}$ component of the $Co^{2+}_{Zn}\,U'(^4A_2)$ ground state. On raising the temperature to 4.2 K lines *a*, *b* and *b*′ increase strongly; these are 'hot' bands originating from the higher $M_S = -\frac{1}{2}$ (*a* and *b*) and $M_S = +\frac{1}{2}$ (*b*′) ground-state levels.

The circularly polarized (c.p.) spectrum of lines L and L′ obtained at 4.2 K in Faraday configuration for $B = 2.71$ T is shown in figure 9 (i). Line L gives rise to four c.p. components, the strongest being lines *a* and *c* which are left (l.) c.p. The right (r.) c.p. components *a*′ and *c*′

arise from the $M_S = +\frac{1}{2}$ and $M_S = +\frac{3}{2}$ ground-state levels respectively. Since component *c* originates from the $U'_\lambda(^4A_2)$ ground-state magnetic subcomponent, the coupling coefficients published by Griffith (1964, table A20) can be used to deduce that the excited state of the L transition at 2.361 eV has E′ symmetry. Weaker c.p. components with a similar sense of splitting are observed from line L′, which is known to have an excited state of U′ symmetry from the stress

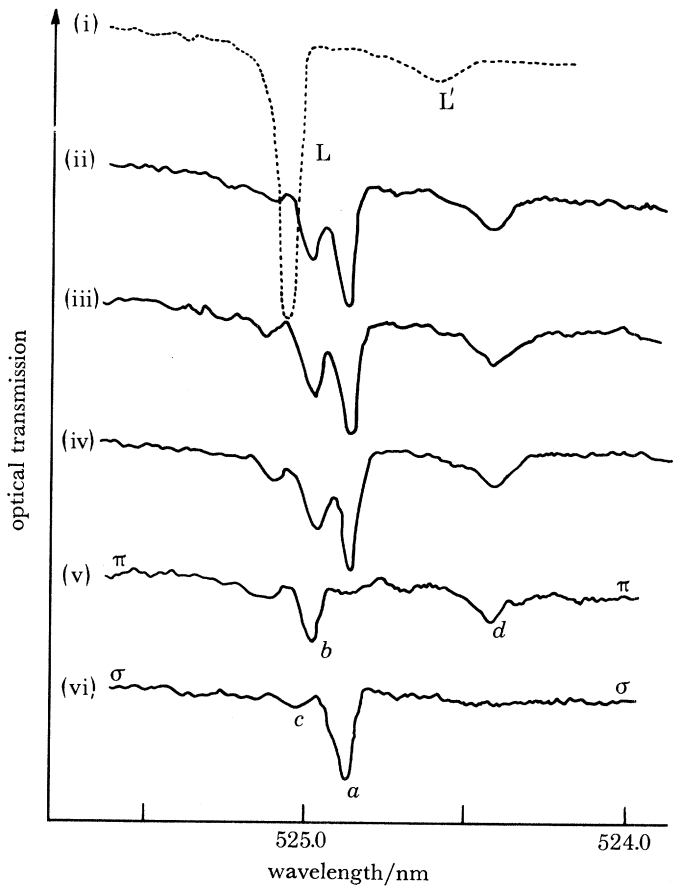

FIGURE 7. Magneto-transmission spectra of the 2.361 eV (L) and 2.363 eV (L′) transitions of ZnSe:Co ($T = 5$ K). The spectra were obtained in Voigt configuration with a transverse-access superconducting solenoid. (i) Zero-field. (ii)–(iv) Unpolarized spectra with a 3.5 T magnetic field applied parallel to the [001] (ii), [111] (iii), and [110] (iv) crystal directions. Within the experimental accuracy, the Zeeman splitting is isotropic. (v)–(vi), Polarized transmission for $B \parallel [001]$. The assignment of the lines labelled (*a*)–(*d*) is given in figure 14.

experiments. This splitting between r.c.p. and l.c.p. is clearly dominated by the magnetic properties of the $[Co^{2+}(d^7)]$ ground state. Figures 9 (ii) and (iii) show the spectra obtained from the higher energy z.p.ls at 2.432 and 2.546 eV. Even with the higher field $B = 6.34$ T the Zeeman splittings are small compared with the line-widths. It is evident, however, that the splitting is in the same sense as for the lower energy lines, with the l.c.p. components moving to higher energy in the magnetic field.

The Zeeman splitting and polarization of lines L and L′ are plotted as a function of magnetic field in figure 10, where the components are labelled to be consistent with figures 7–9. The lines through the experimental points are a numerical fit derived from the theoretical model developed

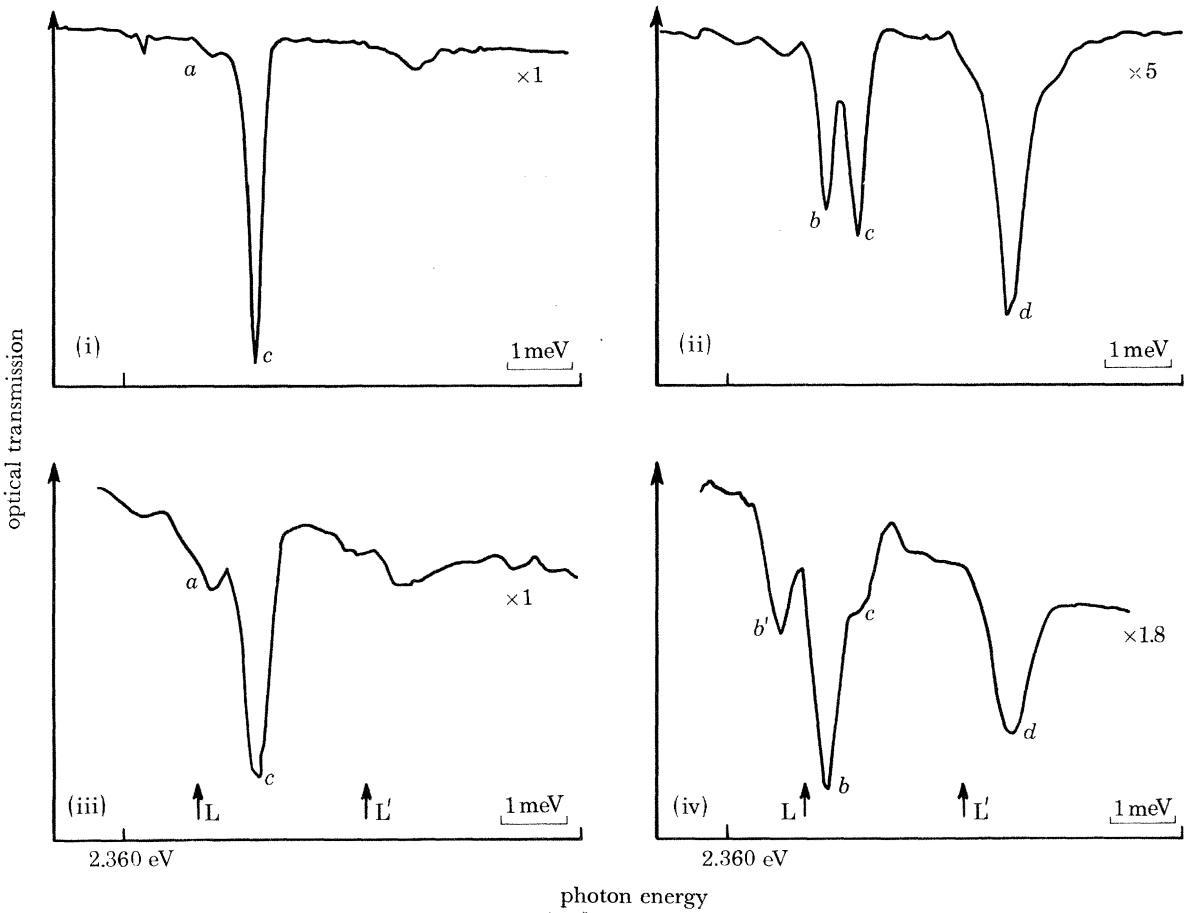

FIGURE 8. Temperature dependence of the polarized magneto-transmission spectra of the 2.361 eV (L) and 2.363 eV (L) transitions of ZnSe:Co. The spectra were obtained at 3.5 T in Voigt configuration by using an electromagnet. The relative detection sensitivities indicated on the spectra are comparable only for a given temperature (1.6 K or 4.2 K). (i) 1.6 K, $E \perp B$; (ii) 1.6 K, $E \parallel B$; (iii) 4.2 K, $E \perp B$; (iv) 4.2 K, $E \parallel B$. The zero-field energies of the L and L′ lines are indicated by arrows in (iii) and (iv). The labelling (a–d) of the lines is explained in the text and in figure 14.

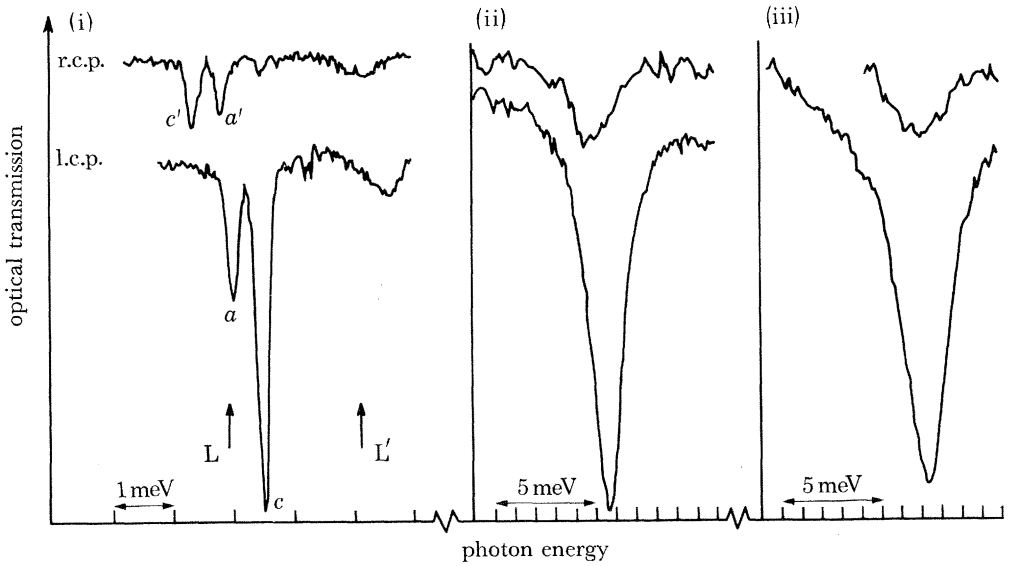

FIGURE 9. Circularly polarized magneto-transmission spectra of the three bands shown in figures 3a–c. The spectra were obtained in Faraday configuration, by using a large-aperture superconducting solenoid (T = 4.2 K). (i) L line (2.361 eV) and L′ line (2.363 eV); B = 2.71 T. The zero-field energies are indicated by arrows. The labelling of the lines is explained in the text and in figure 14. (ii) M line (2.432 eV); B = 6.34 T. (iii) N line (2.546 eV); B = 6.34 T.

in § 5. The $^4A_2(F)$ ground state of Co^{2+}_{Zn} in ZnSe is known to have an almost isotropic Zeeman splitting, with $g = 2.27$ (Ham *et al.* 1960). Using the energy separation between the outer σ and π lines in the splitting diagram for line L the g-value for the 2.361 eV excited state is estimated to have a mean value $g' \approx -0.74$. Thus, the 2.361 eV excited state of E′ symmetry has a *negative* g-value. However, the model developed in § 5 suggests that this excited-state splitting is not linear at higher magnetic fields.

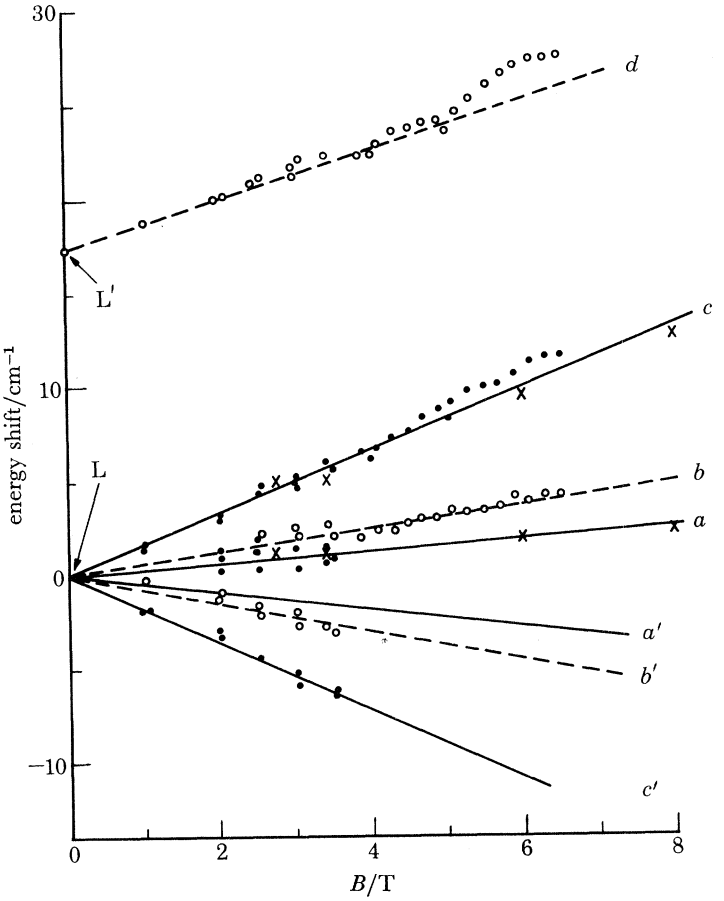

FIGURE 10. Summary of the Zeeman splitting of the 2.361 eV (L) and 2.363 eV (L′) lines of ZnSe:Co. The Zeeman data show the excited state of the L line to have E′ symmetry. Experimental: Voigt configuration, ●(σ), ○(π); Faraday configuration, × (circular polarization). The lines are a numerical fit obtained by using the model developed in § 5 and illustrated in figure 14. The predicted polarizations are: ——, σ; – – –, π.

4. ASSIGNMENTS AND TERMINOLOGY

(*a*) *Possible assignments*

Three possible assignments of the cobalt-induced absorption bands L, M and N were outlined in § 1. The first, (i), a v.b. → impurity c.t. transition was discussed in I and shown to be inconsistent with the weak phonon coupling observed for these transitions. The other two possible assignments, (ii) and (iii), are illustrated *schematically* in figures 11 *a* and *b* respectively, which also indicate the observed c.t. absorption and luminescence transitions. However there

are also serious difficulties associated with (ii). Ligand field theory predicts many states derived from the spin-doublet ($S = \frac{1}{2}$) atomic states of the $Co^{2+}_{Zn}(d^7)$ impurity to lie in the energy range 2.0–2.5 eV (Noras *et al.* 1980). It was pointed out in I that to explain why only three such states are observed in absorption in ZnSe it is necessary to invoke a quasi-resonant interaction with some allowed transition. One strong possibility for such a resonance occurs if the atomic-like spin-doublet states corresponding to lines L, M and N lie above the c.b. minimum, as indicated in

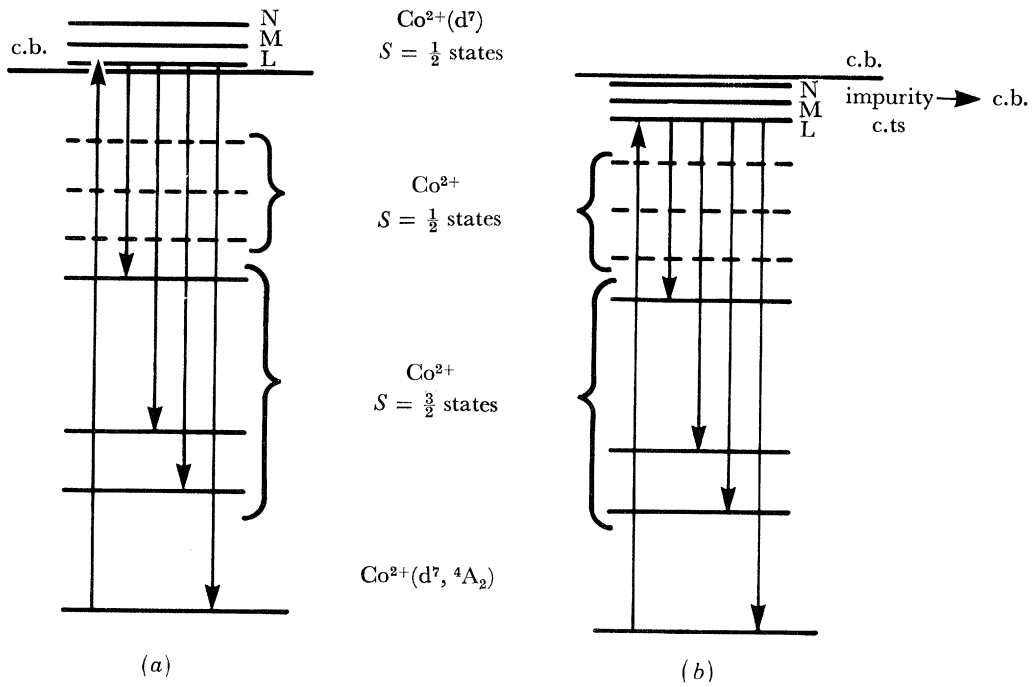

FIGURE 11. Possible schematic models on which to base an assignment of the near-gap absorption bands (L, M, N) of ZnSe:Co. Experimentally observed luminescence transitions are indicated by downward arrows. (*a*) The excited states of the L, M, N transitions are spin-doublet states of the $Co^{2+}_{Zn}(d^7)$ impurity configuration which are resonant with the c.b. and borrow intensity from the continuum absorption. Lower energy spin-doublet states not mixing with the c.b. remain unobservable, and are indicated by broken lines.

(*b*) The excited states of the L, M, N transitions derive from the $Co^{2+}_{Zn}(d^7) \rightarrow [Co^{3+}(d^6)] . e_b$ c.t. excitation, which carries intrinsic oscillator strength. The luminescence occurs from the lowest energy state of this c.t. configuration. The spin-doublet states of $Co^{2+}_{Zn}(d^7)$ are all assumed too weak to be observable.

figure 11*a*. These lines then become observable by borrowing intensity from the continuum absorption, as postulated by Noras *et al.* (1980). The resultant positioning of the $Co^{2+}_{Zn}(d^7)$ ground state relatively close to the v.b. seems to be consistent with recent photocapacitance measurements (Noras *et al.* 1980). According to this model, the spin-doublet states lying below the c.b. edge are assumed not to interact with the ionization continuum and remain too weak to be observed in absorption.

There are however two particular problems with this type of model. The first concerns the observation of luminescence from the lowest state L. The energy gaps between the spin-doublet states of $Co^{2+}_{Zn}(d^7)$ are of the order *ca.* 100 meV in this spectral region (Noras *et al.* 1980), that is only *ca.* 3 LO phonons in ZnSe. It is therefore very surprising that with such small gaps the non-radiative multiphonon relaxation within the $Co^{2+}_{Zn}(d^7)$ doublet manifold should become sufficiently small at level L to allow significant radiative relaxation. The second, rather more

fundamental problem, concerns the line-shapes observed for the three transitions L, M and N. The absorption line-shapes to be expected when a discrete (auto-ionizing) atomic level is degenerate with an ionization continuum are quite well documented (Fano 1961, Fano & Cooper 1968). The line profile can be defined by

$$\sigma(E) = \sigma_c(E)\,[1 + p^2(q^2 - 1 + 2q\epsilon)/(1+\epsilon^2)], \tag{6}$$

where $\sigma_c(E)$ is the absorption cross section in the absence of the auto-ionizing discrete state and

$$\epsilon = (E - E_r)/\tfrac{1}{2}\Gamma, \tag{7}$$

E_r being the theoretical resonance energy and Γ is the line-width, and p, q are parameters determined by wavefunction overlap and relative transition probabilities. Specifically, Fano (1961) gives the following formula for q:

$$q = \frac{(\phi|\,\mathrm{T}\,|i) + P\int \mathrm{d}E'(\phi|\,\mathrm{H}\,|\psi_{E'})\,(\psi_{E'}|\mathrm{T}\,|i)/(E-E')}{\pi(\phi|\,\mathrm{H}\,|\psi_E)\,(\psi_E|\,\mathrm{T}\,|i)}, \tag{8}$$

where ϕ and ψ_E represent the unperturbed discrete state and the unperturbed continuum states respectively, P indicates the 'principal part' of the integral, E' is the energy variable over which the integration is carried out, T is a transition operator and i the initial state of the system. If transitions to the unperturbed discrete state are forbidden, then

$$(\phi|\,\mathrm{T}\,|i) \sim 0, \tag{9}$$

and

$$q \lesssim 1. \tag{10}$$

With this low value of the parameter q, the line-shape is expected to show a marked negative dip in the region of the resonance. Thus, if the unperturbed discrete state does not *itself* introduce significant oscillator strength, it should not produce a large positive absorption feature when in resonance with an ionization continuum from which it borrows oscillator strength to become visible at all.

This analysis can be applied directly to the model in figure 11*a*. Transitions from the $^4A_2(F)$ ground state to the $S = \frac{1}{2}$ doublet states of $Co^{2+}_{Zn}(d^7)$ are spin-forbidden, and because spin remains a 'good' quantum number as discussed in § 3.1 they carry negligible intrinsic oscillator strength. This is the reason that doublet states theoretically predicted to be below the c.b. edge in figure 11*a* are not observed in absorption. However, when such states become resonant and mix with the c.b. continuum they are expected to produce a negative dip or differential line-shape in the continuum absorption. This is clearly not the case for lines L, M and N, which are distinctive, sharp, positive absorption features. The presence and form of absorption lines involving transitions to just these spin-doublet excited states of $Co^{2+}_{Zn}(d^7)$ therefore cannot be readily explained in terms of a model based on assignment (ii), as represented in figure 11*a*.

The remaining possible assignment, (iii) in § 1, does not suffer from the same objections. The model is illustrated in figure 11*b*. The excited state of transition L, described as $[Co^{3+}(d^6)]\,.\,e_b$ in equation (1), then represents the lowest level of this c.t. configuration. Non-radiative relaxation from higher excited states is expected to be rapid, but the substantial electronic reconfiguration needed to cross to the nearby spin-doublet states of $Co^{2+}_{Zn}(d^7)$ may reduce the non-radiative relaxation sufficiently to allow the radiative process to compete. The known upper limit to the lifetime of level L, $\tau_e < 36$ ns, is quite consistent with this interpretation. The weak luminescence

from the 2.361 eV level L is then to be understood as occurring from the lowest excited state of the $[Co^{3+}(d^6)].e_b$ electronic configuration, with non-radiative relaxation into this state from higher states in this configuration as described in § 3.2.

There is also no contradiction between this model (iii) and experimental observations on line-shape and phonon-coupling strength. The impurity → c.b. c.t. excitation can carry intrinsic oscillator strength, thereby producing positive absorption features. The electronic transition also occurs from an anti-bonding d-orbital of the Co_{Zn} impurity to a localized anti-bonding crystal level, i.e. to a localized level derived from the c.b. Thus, there is no gross change in local bonding character of the kind that produces strong phonon coupling in a v.b. → impurity c.t. transition of type (i). It therefore appears that of the three possible assignments listed in § 1, only (iii) is qualitatively consistent with all the experimental absorption and luminescence data. To test this consistency more quantitatively, the model in figure 11*b* has been developed (§ 5) to allow a numerical fit to the absorption and Zeeman data, and a qualitative explanation of the uniaxial stress experiments.

(*b*) *Terminology*

We have used the terms 'v.b. → impurity c.t. transition' and 'impurity → c.b. c.t. transition' to describe the processes (i) and (iii) of § 1. The term 'charge transfer' has been used to emphasize that these are the solid-state analogues of the c.t. excitations familiar from molecular spectroscopy, and particularly from the spectroscopy of discrete inorganic molecular complexes. Two types of transition can occur (McClure 1959):

(*a*) ligand → metal c.t., which is the analogue of (i) and most common for first-row t.m. ions in normal oxidation states;

(*b*) metal → ligand c.t., which is the analogue of (iii) in the sense that the c.b. now plays the part of the low-lying π anti-bonding ligand orbitals usually required to produce such transitions at accessible energies for first-row t.m. ions in normal oxidation states.

Both these processes involve transfer of charge between the central metal ion and the surrounding ligands. The separated electron and hole of course remain closely associated in an isolated chemical complex, because of its discrete molecular nature.

If this concept is translated into the solid state, the term 'charge transfer' becomes useful in denoting an excitation of charge into or out of the unfilled core orbitals of a metal ion impurity, but with the separated electron and hole remaining associated in the excited state and bound by the impurity. The binding may involve both coulombic and central-cell contributions. The term must be qualified to indicate the direction of electron transfer, hence:

type (i): v.b. → impurity c.t., with bound-hole final state

$$[M]^\circ \rightarrow [M]^-.h_b; \tag{11}$$

type (ii): impurity → c.b. c.t., with bound-electron final state

$$[M]^\circ \rightarrow [M]^+.e_b; \tag{12}$$

where the impurity M is assumed neutral with respect to the lattice, like Co^{2+}_{Zn} in ZnSe. The radius of the bound electron or hole, e_b or h_b, will vary with the binding energy and will generally extend beyond the nearest neighbour atoms in the crystal. A threshold for ionization of the excited electron or hole is expected at an energy equal to the sum of the c.t. excitation energy and the binding energy of the relatively weakly bound hole in equation (11), or electron in equation (12).

With these qualifications, the terminology is very useful as a short-hand description of a photoexcitation process which changes the core-orbital occupancy of the impurity producing a bound electron–hole state. The same excited states indicated in (i) and (ii) above can also be formed if the neutral impurity M captures a free exciton by binding either the electron ($\rightarrow [M]^{-}.h_b$) or the hole ($\rightarrow [M]^{+}.e_b$) into a core orbital. If generated in this way the c.t. excited states discussed above might equally be described as deeply bound exciton states. However, these 'bound excitons' are quite different from those normally discussed in the spectroscopy of semiconductors (Dean & Herbert 1979) since the 'deep' binding arises from capture of one particle into an atomic-like core orbital of the impurity, where its character is very different from the valence or c.b. edge states of the host semiconductor.

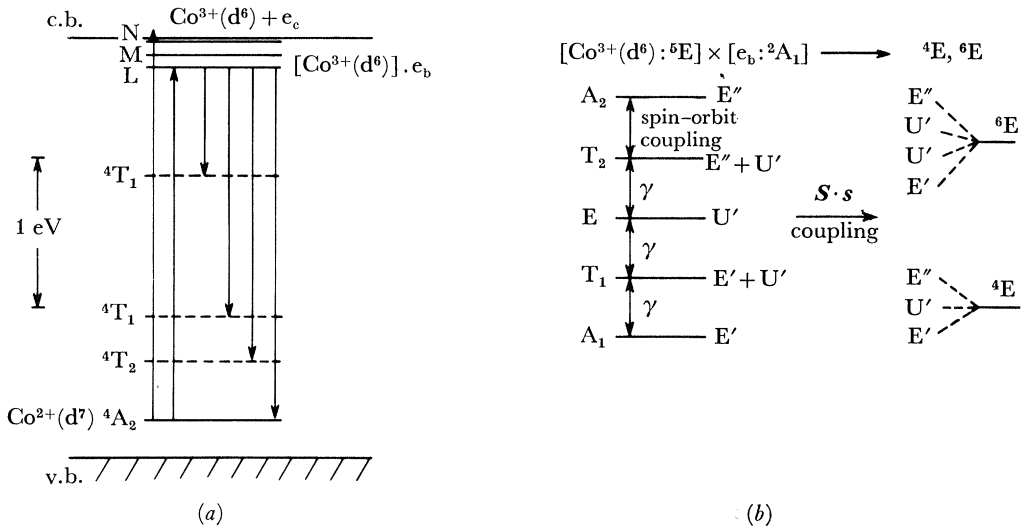

FIGURE 12. (*a*) Energies of the ground state and various excited states of the $Co^{2+}_{Zn}(d^7)$ impurity with respect to the conduction and valence bands of ZnSe. The energy of the $^4A_2(F)$ impurity ground state was set approximately by taking the threshold of the ionization $Co^{2+}_{Zn} \rightarrow Co^{3+}_{Zn} + e_c$ as *ca.* 2.55 eV.

(*b*) Coupling scheme for the lowest energy state of the excited c.t. configuration $[Co^{3+}(d^6, {}^5E)].e_b$. The ^5E state of the residual core $[Co^{3+}(d^6)]$ is split by second-order spin–orbit coupling, and the bound electron e_b in an s-like orbit transforms with $^2A_1(E')$ symmetry. The configuration $[Co^{3+}(d^6, {}^5E)].e_b$ then produces c.t. states of ^4E and ^6E symmetry. The relative energies of these ^4E and ^6E states are determined by interactions represented as a spin–spin coupling term $\boldsymbol{S}\cdot\boldsymbol{s}$ in the Hamiltonian. The final c.t. states transform according to the T_d double-group representations given in the centre of the diagram.

5. A MODEL FOR THE IMPURITY → C. B. CHARGE TRANSFER STATE

For the specific case of ZnSe:Co, the neutral impurity M discussed in the previous section represents the charge state $Co^{2+}_{Zn}(d^7)$. The impurity → c.b. c.t. process is then as given in (1), and illustrated in figure 12*a*. The $Co^{2+}_{Zn}(d^7)$ ground state is set *ca.* 0.25–0.3 eV above the v.b. edge, on the assumption that the broad excitation feature with threshold *ca.* 2.55 eV in figure 2 of I represents the onset of electron ionization discussed in § 4.

We assume that the excited state can be treated as two weakly interacting parts.

(*a*) The residual impurity core $[Co^{3+}(d^6)]$. It also seems reasonable to assume that the lowest-energy ligand-field state of this residual core configuration will be the $^5E(e^3t_2^3)$ state, analogous to the well known case of $Fe^{2+}(d^6)$ (Baranowski *et al.* 1967). It is unlikely that the ligand field

strength will increase for the higher oxidation state [Co^{3+}] sufficiently to make the low spin $^3T_1(e^4t_2^2)$ the lowest energy state.

(*b*) The bound electron e_b. This electron will be assumed to move in an s-like orbit derived largely from the c.b. states at Γ_c. Thus, this electron has $^2A_1$ symmetry.

The overall symmetry of the lowest-energy c.t. excited states is then given by the direct product:

$$[Co^{3+}(d^6)]\,(^5E) \times e_b(^2A_1) \rightarrow [Co^{3+}(d^6)]\,.\,e_b(^4E + {}^6E), \tag{13}$$

i.e. the lowest energy c.t. states are a spin-quartet ($S = \frac{3}{2}$) and a spin-sextet ($S = \frac{5}{2}$) of E (twofold degenerate) orbital symmetry.

The degeneracy of these c.t. states will be lifted by two principal interactions. The first is the spin–orbit coupling $\mathscr{H}_{SO}$, which will, however, act only in second order since the E orbital state possesses no first-order orbital moment. The second is the coupling between the excited electron and the residual impurity core, $\mathscr{H}_c$. We represent this coupling as the sum of a symmetric spin-independent term and an exchange term which is introduced as a simple spin–spin interaction term of the form $\mathscr{H}_{EX} \propto \boldsymbol{S}\cdot\boldsymbol{s}$, where $|\boldsymbol{S}| = 2$ the total spin-vector of the [$Co^{3+}(d^6)$ (^5E)] core and $|\boldsymbol{s}| = \frac{1}{2}$ is the spin of the bound electron e_b. The ultimate test of these various assumptions is of course whether the model derived from them is able to give a satisfactory fit to the experimental data.

By using a perturbation approach, the two parts of the excited state can be coupled together in different ways. If $\mathscr{H}_{EX} > \mathscr{H}_{SO}$ the c.t. configuration will split into a ^4E and a ^6E state, which will then split further under the spin–orbit coupling:

$$\left.\begin{aligned} {}^4E &\rightarrow E' + E'' + U', \\ {}^6E &\rightarrow E' + E'' + 2U'. \end{aligned}\right\} \tag{14}$$

If, however, $\mathscr{H}_{SO} > \mathscr{H}_{EX}$ the spin–orbit coupling will lift the degeneracy of the residual core, and the spin–orbit components of the [$Co^{3+}(d^6)$ (^5E)] state may couple separately to the excited electron $e_b(E')$ via the exchange interaction:

$$\left.\begin{aligned} {}^5E(d^6) &\rightarrow A_1 + A_2 + E + T_1 + T_2, \\ A_1 \times E' &\rightarrow E', \\ A_2 \times E' &\rightarrow E'', \\ E \times E' &\rightarrow U', \\ T_1 \times E' &\rightarrow E' + U', \\ T_2 \times E' &\rightarrow E'' + U'. \end{aligned}\right\} \tag{15}$$

These limiting coupling schemes are illustrated in figure 12*b*. However, in fitting to the experimental data, we shall treat these two interactions equally and use a matrix diagonalization technique to obtain the eigenvectors and eigenvalues.

Since detailed experimental data are available only for the absorption band with origin at 2.361 eV (L), we shall parametrize the model to fit the properties of this band. Of course, if the model is finally to be acceptable it must also offer a consistent assignment for the higher energy absorption features with z.p.ls at 2.432 eV (M) and 2.546 eV (N). It will become evident later that the two terms $\mathscr{H}_{SO}$ and $\mathscr{H}_{EX}$ are sufficient to fit the known symmetry (E′) and the negative *g*-value of the 2.361 eV (L) excited state. However, with only these terms in the Hamiltonian, it is difficult to account for the weaker sharp feature L′ at 2.363 eV. The excited state of the L′

PHILOSOPHICAL TRANSACTIONS OF THE ROYAL SOCIETY A MATHEMATICAL, PHYSICAL & ENGINEERING SCIENCES

transition is known from the stress measurements to have U′ symmetry, and a highly anisotropic splitting pattern. One possibility is that the excited states of both the L and L′ transitions are purely electronic, and derive from a small perturbation (ligand field, spin–orbit or spin–spin), of a state of higher (sixfold) degeneracy. However, the relative weakness of the L′ absorption, although it has the excited state of greater degeneracy, argues against such an explanation.

A second possibility is that the excited state of the L′ transition is vibronic in origin, and represents a phonon mode pushed to low energy via a Jahn–Teller (J–T) interaction. The absorption intensity in this line would then be determined by the strength of the J–T mixing. Evidence for a J–T interaction is now well established for both the $d^6(^5E)$ configuration of Fe^{2+} (Vallin 1970; West *et al.* 1980; Vogel & Rivera-Iratchet 1980) and for the d^7 configuration of Co^{2+} (Uba & Baranowski 1978; Hennel & Uba 1978). To fit the properties of the L′ transition in addition to L we shall therefore include the possibility of a vibronic interaction by adding a J–T term $\mathscr{H}_{JT}$ to the model Hamiltonian. This introduces two extra parameters, an effective phonon frequency and a J–T coupling energy.

The model Hamiltonian therefore has the form:

$$\begin{aligned}\mathscr{H} &= \mathscr{H}_{SO}+\mathscr{H}_{C}+\mathscr{H}_{JT}\\ &= \mathscr{H}_{SO}+\mathscr{H}_{O}+\mathscr{H}_{EX}+\mathscr{H}_{JT},\end{aligned} \tag{16}$$

where $\mathscr{H}_O$ is a totally symmetric term adding a constant energy to the electron binding.

In the following sections we consider first the basis wavefunctions and then each of these energy terms separately. In §5.5 we construct and diagonalize the matrices for the c.t. states of E′, E″ and U′ symmetry to obtain the eigenvalues and eigenvectors. Finally a Zeeman energy term $\mathscr{H}_Z$ will be added to fit the magnetic field data.

(*a*) *The basis wavefunctions*

The spin–orbit and J–T energies are dominated by interactions within the $[Co^{3+}(d^6)\ (^5E)]$ core configuration. It is therefore useful to use as an electronic basis set the product wavefunctions $|d^6(^5E,\Gamma)\,.\,s(^2A_1,E');\Gamma'\gamma'\rangle$ where Γ is a spin–orbit component of the $[Co^{3+}(d^6)\ (^5E)]$ residual core, Γ′ is the double-group representation of the product c.t. state, and γ′ a particular component. With the use of Griffith's (1964) coupling coefficients, these product states can be expressed as linear combinations of the spin–orbit components of the ^4E and ^6E c.t. states (for brevity the symbols ^5E and $^2A_1$ are omitted from the following):

$$|d^6(A_1)\,.\,s(E')\,;E'\alpha'\rangle = -\sqrt{\tfrac{3}{5}}\,|(^6E)\,E'\alpha\rangle+\sqrt{\tfrac{2}{5}}\,|(^4E)\,E'\alpha'\rangle, \tag{17}$$

$$|d^6(T_1)\,.\,s(E')\,;E'\alpha'\rangle = -\sqrt{\tfrac{2}{5}}\,|(^6E)\,E'\alpha'\rangle-\sqrt{\tfrac{3}{5}}\,|(^4E)\,E'\alpha'\rangle, \tag{18}$$

$$|d^6(A_2)\,.\,s(E')\,;E''\alpha''\rangle = -\sqrt{\tfrac{3}{5}}\,|(^6E)\,E''\alpha''\rangle+\sqrt{\tfrac{2}{5}}\,|(^4E)\,E''\alpha''\rangle, \tag{19}$$

$$|d^6(T_2)\,.\,s(E')\,;E''\alpha''\rangle = -\sqrt{\tfrac{2}{5}}\,|(^6E)\,E''\alpha''\rangle-\sqrt{\tfrac{3}{5}}\,|(^4E)\,E''\alpha''\rangle, \tag{20}$$

$$|d^6(T_1)\,.\,s(E')\,;U'_\kappa\rangle = -\sqrt{\tfrac{1}{2}}\,|(^6E)\,U'_{1\kappa}\rangle-\sqrt{\tfrac{1}{5}}\,|(^6E)\,U'_{2\kappa}\rangle-\sqrt{\tfrac{3}{10}}\,|(^4E)\,U'_\kappa\rangle, \tag{21}$$

$$|d^6(E)\,.\,s(E')\,;U'_\kappa\rangle = \sqrt{\tfrac{3}{5}}\,|(^6E)\,U'_{2\kappa}\rangle-\sqrt{\tfrac{2}{5}}\,|(^4E)\,U'_\kappa\rangle, \tag{22}$$

$$|d^6(T_2)\,.\,s(E')\,;U'_\kappa\rangle = -\sqrt{\tfrac{1}{2}}\,|(^6E)\,U'_{1\kappa}\rangle+\sqrt{\tfrac{1}{5}}\,|(^6E)\,U'_{2\kappa}\rangle+\sqrt{\tfrac{3}{10}}\,|(^4E)\,U'_\kappa\rangle, \tag{23}$$

where $|(^4\mathrm{E})\,\Gamma'\rangle$ and $|(^6\mathrm{E})\,\Gamma'\rangle$ c.t. states are products of spin and orbital E state functions, $|SM_S\rangle\,|LM_L\rangle$:

$$|(^4\mathrm{E})\,\mathrm{E}'\alpha'\rangle = \tfrac{1}{\sqrt{2}}\,|\tfrac{3}{2}\,\tfrac{1}{2}\rangle\,|\mathrm{E}\theta\rangle + \tfrac{1}{\sqrt{2}}\,|\tfrac{3}{2}\,-\tfrac{3}{2}\rangle\,|\mathrm{E}\varepsilon\rangle, \tag{24}$$

$$|(^6\mathrm{E})\,\mathrm{E}'\alpha'\rangle = \tfrac{\sqrt{5}}{2\sqrt{3}}\,|\tfrac{5}{2}\,\tfrac{5}{2}\rangle\,|\mathrm{E}\varepsilon\rangle + \tfrac{1}{\sqrt{2}}\,|\tfrac{5}{2}\,\tfrac{1}{2}\rangle\,|\mathrm{E}\theta\rangle + \tfrac{1}{2\sqrt{3}}\,|\tfrac{5}{2}\,-\tfrac{3}{2}\rangle\,|\mathrm{E}\varepsilon\rangle, \tag{25}$$

$$|(^4\mathrm{E})\,\mathrm{E}''\alpha''\rangle = -\tfrac{1}{\sqrt{2}}\,|\tfrac{3}{2}\,-\tfrac{3}{2}\rangle\,|\mathrm{E}\theta\rangle + \tfrac{1}{\sqrt{2}}\,|\tfrac{3}{2}\,\tfrac{1}{2}\rangle\,|\mathrm{E}\varepsilon\rangle, \tag{26}$$

$$|(^6\mathrm{E})\,\mathrm{E}''\alpha''\rangle = -\tfrac{\sqrt{5}}{2\sqrt{3}}\,|\tfrac{5}{2}\,\tfrac{5}{2}\rangle\,|\mathrm{E}\theta\rangle + \tfrac{1}{\sqrt{2}}\,|\tfrac{5}{2}\,\tfrac{1}{2}\rangle\,|\mathrm{E}\varepsilon\rangle - \tfrac{1}{2\sqrt{3}}\,|\tfrac{5}{2}\,-\tfrac{3}{2}\rangle\,|\mathrm{E}\theta\rangle, \tag{27}$$

$$|(^4\mathrm{E})\,\mathrm{U}'_\kappa\rangle = \tfrac{1}{\sqrt{2}}\,|\tfrac{3}{2}\,\tfrac{3}{2}\rangle\,|\mathrm{E}\theta\rangle + \tfrac{1}{\sqrt{2}}\,|\tfrac{3}{2}\,-\tfrac{1}{2}\rangle\,|\mathrm{E}\varepsilon\rangle, \tag{28}$$

$$|(^6\mathrm{E})\,\mathrm{U}'_{1\kappa}\rangle = -\tfrac{\sqrt{5}}{\sqrt{6}}\,|\tfrac{5}{2}\,\tfrac{3}{2}\rangle\,|\mathrm{E}\theta\rangle + \tfrac{1}{\sqrt{6}}\,|\tfrac{5}{2}\,-\tfrac{5}{2}\rangle\,|\mathrm{E}\theta\rangle, \tag{29}$$

$$|(^6\mathrm{E})\,\mathrm{U}'_{2\kappa}\rangle = -\tfrac{1}{2\sqrt{3}}\,|\tfrac{5}{2}\,\tfrac{3}{2}\rangle\,|\mathrm{E}\theta\rangle - \tfrac{1}{\sqrt{2}}\,|\tfrac{5}{2}\,-\tfrac{1}{2}\rangle\,|\mathrm{E}\varepsilon\rangle - \tfrac{\sqrt{5}}{2\sqrt{3}}\,|\tfrac{5}{2}\,-\tfrac{5}{2}\rangle\,|\mathrm{E}\theta\rangle. \tag{30}$$

It is worth noting here that the c.t. state of E′ symmetry derived from the spin-quartet state, i.e. $|(^4\mathrm{E})\,\mathrm{E}'\alpha'\rangle$, has a negative g-value arising from the $|\tfrac{3}{2}\,-\tfrac{3}{2}\rangle$ spin component in the wavefunction. This state therefore has approximately the properties required for the excited state of the 2.361 eV (L) transition. The final vibronic states required for solution of the J–T problem are obtained as products of this electronic basis set with vibrational wavefunctions of the appropriate symmetry (§ 5 (*d*)).

(*b*) *The spin–orbit coupling*, $\mathscr{H}_{\mathrm{SO}}$

In calculating the effects of the spin–orbit operator within the c.t. product states (equations (17)–(23)), a great simplification results from the fact that $\mathscr{H}_{\mathrm{SO}}$ is a sum over one-electron operators:

$$\mathscr{H}_{\mathrm{SO}} = \sum_i \boldsymbol{s}_i \cdot \boldsymbol{l}_i, \tag{31}$$

where $\boldsymbol{s}_i$ and $\boldsymbol{l}_i$ are the spin and orbital angular momentum operators for electron i. When the properly antisymmetrized wavefunction is represented as a product of functions that have no one-electron orbitals in common, Griffith (1962) has shown that the matrix elements of a one-electron operator can be factorized into a sum over matrix elements involving the component functions separately. The general matrix element for the configurationally diagonal c.t. product states then becomes

$$\begin{aligned}\langle \mathrm{d}^6(^5\mathrm{E},\Gamma)\,.\,\mathrm{s}(^2\mathrm{A}_1,\mathrm{E}')\,;\Gamma'\gamma'|\,\mathscr{H}_{\mathrm{SO}}\,|\mathrm{d}^6(^5\mathrm{E},\Gamma'')\,.\,\mathrm{s}(^2\mathrm{A}_1,\mathrm{E}')\,;\Gamma'\gamma'\rangle \\ = \langle \mathrm{d}^6(^5\mathrm{E},\Gamma)|\,\mathscr{H}_{\mathrm{SO}}\,|\mathrm{d}^6(^5\mathrm{E},\Gamma'')\rangle\delta_{\Gamma\Gamma''} + \langle \mathrm{s}(^2\mathrm{A}_1,\mathrm{E}')|\,\mathscr{H}_{\mathrm{SO}}\,|\mathrm{s}(^2\mathrm{A}_1,\mathrm{E}')\rangle \\ = \langle \mathrm{d}^6(^5\mathrm{E},\Gamma)|\,\mathscr{H}_{\mathrm{SO}}\,|\mathrm{d}^6(^5\mathrm{E},\Gamma)\rangle,\end{aligned} \tag{32}$$

i.e. the spin–orbit splitting of the c.t. product states in equations (17)–(23) is determined by the splitting of the $\mathrm{d}^6(^5\mathrm{E})$ core states. The problem then becomes analogous to the well known case of $\mathrm{Fe}^{2+}(\mathrm{d}^6,{}^5\mathrm{E})$.

The spin–orbit coupling operator can in general be expressed in the form of an operator-equivalent, $\boldsymbol{Q}$, which is a sum over irreducible products of degree 0 (Griffith 1962):

$$\boldsymbol{Q} = \sum_g a(g)\,[\boldsymbol{S}^{(g)} \times \boldsymbol{L}^{(g)}]^0, \tag{33}$$

where $\boldsymbol{S}^{(g)}$ and $\boldsymbol{L}^{(g)}$ are themselves irreducible products of degree g involving g spin vectors and g orbital vectors respectively. The term in $g = 0$ produces a uniform shift of levels, and the term in $g = 1$ gives the first-order spin–orbit coupling energy. For a given atomic state $|SL\rangle$ the terms

in $g = 2$ have the form required to include both the second-order spin–orbit corrections and the first-order spin–spin coupling energies. In the T_d point group of a zinc-blende crystal, and for an E orbital state only, this operator reduces to

$$\boldsymbol{Q} = a(A_1)\,[\boldsymbol{S}^{(A_1)} \times \boldsymbol{L}^{(A_1)}]^{A_1} + a(E)\,[\boldsymbol{S}^{(E)} \times \boldsymbol{L}^{(E)}]^{A_1}. \tag{34}$$

An $|\boldsymbol{S}| = 2$ spin vector spans the representations $E + T_2$ in the T_d point group. Therefore, from symmetry considerations alone, a total of four spin-related parameters could be required to describe the spin–orbit splitting of the $d^6(^5E)$ state, consistent with the experimental observations that the spacings between the five spin–orbit components of the $Fe^{2+}(d^6)$ ground state are not exactly equal (Ham & Slack 1971; West *et al.* 1980). However, to a first approximation the levels can be considered as equally spaced, which is equivalent to assuming that the $E(|\boldsymbol{S}| = 2)$ and $T_2(|\boldsymbol{S}| = 2)$ functions are pure free-spin $|\boldsymbol{S}| = 2$ functions. Only one parameter is then required to describe the spin–orbit splitting of the c.t. product states. Accordingly, we shall represent this splitting by the single energy parameter γ as indicated on the left-hand side of figure 12*b*.

(*c*) *The coupling between the core and excited electron, $\mathscr{H}_C$*

As previously discussed the binding between the residual core $[C_0^{3+}(d^6, {}^5E)]$ and the excited electron e_b is assumed to have the form:

$$\mathscr{H}_C = \mathscr{H}_O + \mathscr{H}_{EX}, \tag{35}$$

where $\mathscr{H}_O$ is a symmetric, spin-independent interaction and $\mathscr{H}_{EX}$ a relatively weak exchange interaction. The latter is introduced in the simple form

$$\mathscr{H}_{EX} = \tfrac{2}{3}D\boldsymbol{S}\cdot\boldsymbol{s}, \tag{36}$$

where

$$\boldsymbol{S} = \sum_{i=1}^{6} \boldsymbol{s}_i \tag{37}$$

is the total spin of the residual core, and $\boldsymbol{s}$ the spin of the bound electron. The exchange operator in (36) is diagonal in both total spin $\boldsymbol{S}' = \boldsymbol{S} + \boldsymbol{s}$ and within the T_d double-group representations of the spin–orbit components of the c.t. product states. With the operator in this form the ^4E and ^6E c.t. states are split by $-D$ and $+\frac{2}{3}D$ respectively. The matrices of the exchange interactions in the product basis are

$\Gamma' = E'$	$\lvert d^6(A_1).s(E')\rangle$	$\lvert d^6(T_1).s(E')\rangle$
	0	$\frac{2}{\sqrt{6}}D$
	$\frac{2}{\sqrt{6}}D$	$-\frac{1}{3}D$

(38)

$\Gamma' = E''$	$\lvert d^6(A_2).s(E')\rangle$	$\lvert d^6(T_2).s(E')\rangle$
	0	$\frac{2}{\sqrt{6}}D$
	$\frac{2}{\sqrt{6}}D$	$-\frac{1}{3}D$

(39)

$\Gamma' = U'$	$\lvert d^6(T_1).s(E')\rangle$	$\lvert d^6(E).s(E')\rangle$	$\lvert d^6(T_2).s(E')\rangle$
	$\frac{1}{6}D$	$-\frac{2\sqrt{3}}{6}D$	$\frac{1}{2}D$
	$-\frac{2\sqrt{3}}{6}D$	0	$\frac{2\sqrt{3}}{6}D$
	$\frac{1}{2}D$	$\frac{2\sqrt{3}}{6}D$	$\frac{1}{6}D$

(40)

The total interaction energy between the core and e_b is obtained within the model by adding a constant diagonal term arising from $\mathscr{H}_O$ to these matrices. The usefulness of assuming the interaction to be separable in this way will ultimately be tested by comparison of the model predictions with the experimental data.

(*d*) *The Jahn–Teller coupling*, $\mathscr{H}_{JT}$

As stated in the introduction to § 5, the c.t. state spin–orbit and exchange interactions discussed above are sufficient to account for the measured properties of the L absorption line at 2.361 eV. The weaker L′ line at 2.363 eV, on the other hand, is probably vibronic in origin, so that an electron–phonon interaction must be introduced into the model. We shall treat this J–T problem as separable into a sum of two terms, involving the vibronic interactions for the $[Co^{3+}(d^6, {}^5E)]$ core and the bound electron e_b. This is a reasonable simplification, since the J–T coupling is dominated by individual electron–ion interactions, so that to a good approximation the matrix elements of $\mathscr{H}_{JT}$ should be factorizable in a manner analogous to that for the element of $\mathscr{H}_{SO}$. We are therefore neglecting small energy shifts associated with phonon-induced mixing of the s-like wavefunction of e_b with the core d-orbitals; however such mixing is clearly not zero since it leads to the non-radiative relaxation of the excited $[Co^{3+}(d^6, {}^5E)]\,.\,e_b$ c.t. configuration into the higher d^7 excited states of the Co^{2+}_{Zn} configuration, which must occur to account for the p.l.e. spectra in figure 3.

With these assumptions the problem reduces to a calculation involving interactions within the $d^6({}^5E)$ core alone, since the J–T operator has a zero matrix element for the orbitally non-degenerate bound-electron state, $e_b({}^2A_1)$. The calculation is analogous to the treatment of the J–T interaction in $Fe^{2+}(d^6, {}^5E)$, discussed at length by Vallin (1970). For an E orbital state only phonons projecting e symmetry modes in the T_d impurity point group can give rise to a first-order J–T interaction. The operator then has the form:

$$\mathscr{H}_{JT} = V[q_\theta U_\theta + q_\varepsilon U_\varepsilon], \tag{41}$$

where θ, ε are the components of the E(e) electronic (vibrational) state, U_θ, U_ε are orbital operators and q_θ, q_ε are linear combinations of ion displacements possessing the appropriate symmetry. We shall assume a single active mode of energy $\hbar\omega_e$.

The J–T matrix within the $d^6({}^5E)$ configuration is diagonal in the spin functions $E(|\boldsymbol{S}| = 2)$ and $T_2(|\boldsymbol{S}| = 2)$, but introduces off-diagonal terms between the spin–orbit components of the c.t. excited state. Since only the properties of the two lowest-energy states, giving the lines L and L′, are of detailed interest, only zero-, one- and two-phonon states have been included in the calculation. The two-phonon states have symmetries determined by the symmetric direct product $[e \times e]^S \rightarrow a_1 + e$. The overall vibronic states which form the basis for diagonalization of the system Hamiltonian, equation (16), can be obtained as linear combinations of products of the c.t. electronic states, equations (17)–(23), and the appropriate phonon states, by using the coupling coefficients given by Griffith (1964). The J–T matrix can be calculated from this basis by following the method of Vallin (1970).

(*e*) *Diagonalization of the Hamiltonian*

The total Hamiltonian $\mathscr{H}$, given by equation (16), is diagonal in the *vibronic* states which transform according to the T_d double-group representations E′, E″ and U′. The total matrix corresponding to each of these representations is obtained by adding the matrices for the individual terms $\mathscr{H}_{SO}$, $\mathscr{H}_C$ and $\mathscr{H}_{JT}$, calculated in the vibronic basis states discussed in the

previous section. In addition a Zeeman energy term $\mathscr{H}_Z$ must be included to allow calculation of the magnetic splitting pattern:

$$\mathscr{H}_Z = \beta(\boldsymbol{L} + 2\boldsymbol{S}) \cdot \boldsymbol{H}. \tag{42}$$

As an example the matrix of the E′α′ vibronic basis set is given in the Appendix. With the truncation at two-phonon states the E′ and E″ matrices are of dimension 10×10, and the U′ matrix is 20×20.

It was noted in § 3 (*a*) that spin remains a reasonably 'good' quantum number for the $Co^{2+}_{Zn}(d^7)$ impurity, in the sense that only spin-allowed transitions from the $^4A_2(F)$ ground state to the spin-quartet ligand-field excited states are readily observable in optical absorption. This is true even for the weak $^4A_2(F) \rightarrow {}^4T_2(F)$ transition, which is dipole-forbidden in T_d symmetry where the dipole moment operator transforms as T_2. The intensity in this otherwise forbidden transition results largely from spin–orbit admixture of the $^4T_1(F)$ and $^4T_1(P)$ states into $^4T_2(F)$. To estimate relative absorption strengths in the c.t. transitions from our model we shall assume that analogous selection rules hold for the impurity → c.b. c.t. transitions. Significant optical absorption is therefore only associated with components of the $^4A_2(F) \rightarrow {}^4E$ zero-phonon c.t. transition, the $^4A_2(F) \rightarrow {}^6E$ process being effectively spin-forbidden. The $^4A_2(F) \rightarrow {}^4E$ electronic transition is itself dipole-forbidden, but is assumed to acquire oscillator strength by admixture of $^4T_1$ excited states. Such $^4T_1$ states would arise for example from the higher lying $[Co^{3+}(d^6, {}^5T_2)].e_b$ c.t. configuration, and from the energetically neighbouring (but not overlapping) continuum states resulting from ionization of e_b.

The vibronic matrices have been diagonalized to give the eigenvalues and eigenvectors for the c.t. states of E′, E″ and U′ symmetry. The relative line strengths in zero magnetic field were calculated from the square of the ^4E state coefficient in each eigenvector, with $\boldsymbol{H} = 0$. The way in which the predicted band-shape varies with the model parameters is illustrated in figure 13. The spin–orbit parameter and phonon energy were set at $\gamma = 1$, $\hbar\omega_E = 0.5$, in figure 13*a*, with $D = V = 0$. The predicted intensity is associated with purely electronic transitions and is distributed over the energies of the spin–orbit components of the $[Co^{3+}(d^6, {}^5E)]$ residual core. The exchange coupling is turned on in figure 13*b*, with a value of the parameter $D = 0.55$. The positive value given to this parameter stabilizes the ^4E c.t. state compared with ^6E, so that the absorption strength generally moves to lower energy. Additionally, the degeneracy of the E′ and U′ c.t. states arising from the $|d^6(T_1)\rangle$ component, and of the E″ and U′ states from $|d^6(T_2)\rangle$, are lifted. The effect of the finite exchange interaction is to produce an origin line of E′ symmetry with significant ^4E character. This line is therefore both strong in absorption and possesses a negative *g*-value, as for the L transition. The value $D = 0.55$ is used here because it gives a good fit to the Zeeman data.

Figures 13*c–e* illustrate the effect of increasing J–T interaction in the model. The higher energy electronic states mix strongly with the phonon states, but the origin line is relatively unaffected. The lowest energy phonon state at energy $\hbar\omega_E = 0.5$ in figure 13*a* and labelled L′ in figures 13*c–e* has U′ symmetry; this vibronic state moves rapidly to lower energy as V increases, gaining intensity by admixture of higher energy electronic states of U′ symmetry. This transition therefore has some of the properties required of the L′ line.

Figure 13 is illustrative in the sense that no attempt has been made to optimize for 'best-fit' values of the parameters. Nevertheless it is interesting to compare the band-shape predicted by the model with the experimental absorption band. This is done in figure 1*a*, where the abscissa

of figure 13*e* has been scaled to fit the energy separation between the L and L′ lines. This scaling fixes the energy of the spin–orbit parameter as $\gamma = 56\,\mathrm{cm}^{-1}$. Only the strongest lines in figure 13*e* are reproduced in figure 1*a*, but clearly the predicted absorption energies are in rather good agreement with those absorption features noted in §3 (*a*) which do not correspond to phonon density-of-states peaks.

The Zeeman energy level diagram can be calculated as a function of increasing magnetic field through the term $\mathscr{H}_Z$ in the Hamiltonian. The splitting of the two lowest-energy excited states, of

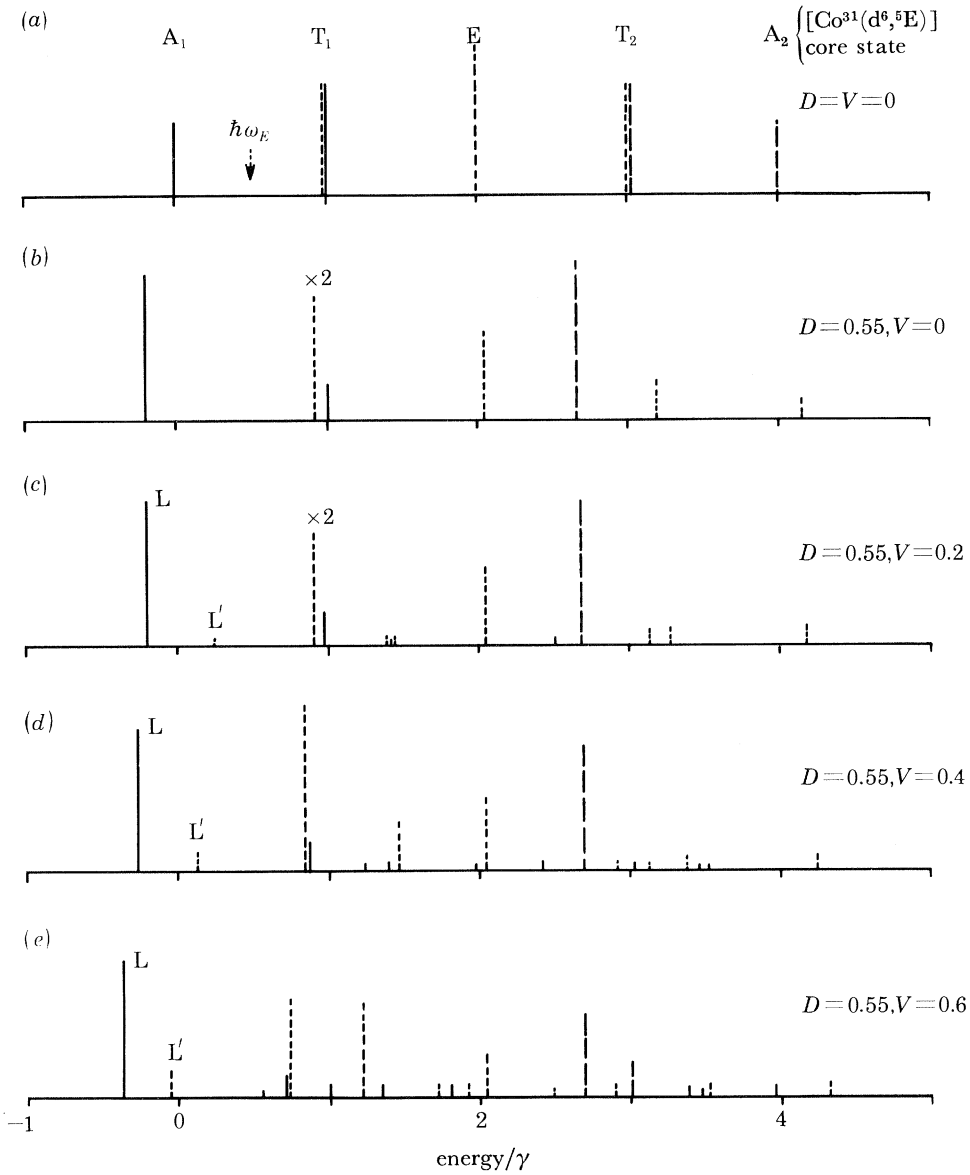

FIGURE 13. Absorption line-shape for the $Co^{2+}_{Zn}(d^7) \rightarrow [Co^{3+}(d^6, {}^5E)].e_b$ c.t. excitation of ZnSe:Co, predicted from the model developed in §5. Only components of the $^4A_2 \rightarrow {}^4E$ c.t. excitation carry significant oscillator strength. (*a*) Spin–orbit coupling only, $\gamma = 1$. The J–T active mode has energy $\hbar\omega_E = 0.5$. (*b*) Inclusion of spin-dependent exchange coupling, $D = 0.55$. (*c*)–(*e*) Inclusion of increasing J–T interaction, $V > 0$. The symmetries of the excited states of the various transitions are E′ (——); E″ (– – –); U′ (------). (The lines marked × 2 should be doubled to obtain the correct relative intensities.)

symmetry E′ and U′, is given in the upper part of figure 14. The parameters used are listed in the caption. The bottom of this figure shows the isotropic Zeeman splitting of the $Co^{2+}_{Zn}(d^7)\,^4A_2(F)$ ground state, with $g = 2.27$ (Ham *et al.* 1960). The predicted splitting pattern, including polarization, is indicated by the lines in figure 10, where there is evidently excellent quantitative agreement with the experimental data (figures 7–10). Once again, no attempt has been made to optimize this fit by least-squares analysis. Five of the six predicted lines for the $^4A_2 \rightarrow E'$ (L) transition are observed, but for the weaker $^4A_2 \rightarrow U'$ (L′) transition only one π-polarized line (*d*)

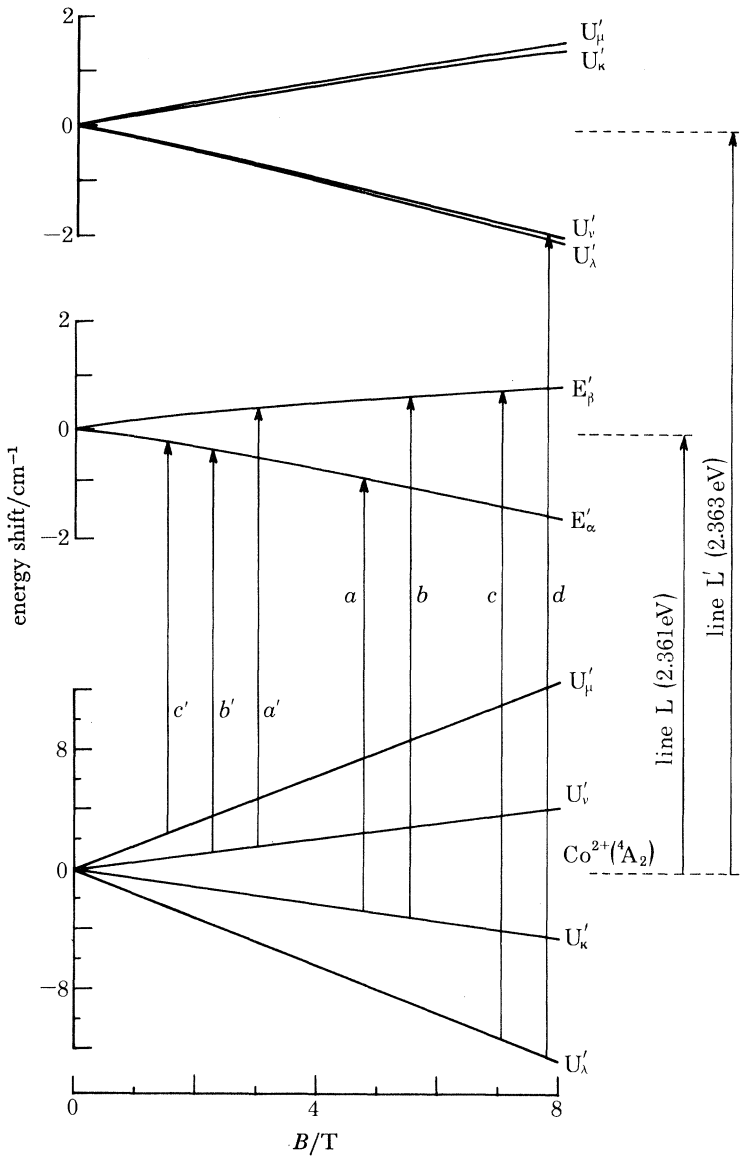

FIGURE 14. Magnetic-field energy level diagram and assignment of Zeeman components for the 2.361 eV (L) and 2.363 eV (L′) lines of ZnSe:Co. The lower part of the diagram gives the ground-state splitting for $Co^{2+}_{Zn}(d^7)$ with $g = 2.27$. The splittings of the excited states of E′ and U′ symmetry are predicted by the model of §5 with the parameters $\gamma = 56\ cm^{-1}$, $\hbar\omega_E = 28\ cm^{-1}$, $D = 30.8\ cm^{-1}$ and $V/\alpha = 33.6\ cm^{-1}$. The negative *g*-value for the E′ state and the unusual splitting of the U′ state are discussed in the text. *Note* the ordinate-scale expansion for the excited-state splittings compared with that for the ground state.

originating from the $^4A_2(U'_\lambda)$ Zeeman ground state is readily observable. From Griffith's (1964 tables of coupling coefficients, this dominant π-polarization of the L′ transition is predicted if the intensity arises primarily from mixing with a $^4T_1(\frac{5}{2}U')$ allowed state. Weaker σ-polarized transitions from this lowest-energy, ground-state magnetic subcomponent to the U'_μ and U'_κ components of the L′ line would be expected to occur at higher energy, but with an energy shift rather smaller than the line-width. In fact both the Voigt and the Faraday configuration data in figures 8 and 9 show weak σ-polarized components which possibly represent those transitions.

Two points should be noted from figure 14. First, the excited-state splittings are predicted to be slightly nonlinear in the magnetic field. This arises because the matrix elements of the exchange operator $\mathscr{H}_{EX}$ and of $\mathscr{H}_Z$ may differ in phase for particular pairs of basis functions. There is therefore a quantum-mechanical interference effect between these operators in the model. However, with the parameters giving a good fit to the Zeeman pattern the predicted non-linearity is too small to be detectable experimentally. Also, the excited state of U′ symmetry at 2.363 eV splits mainly as a doublet, with a small subsidiary splitting into four components. This unusual splitting arises because the wavefunction of the U′ excited state has dominant contributions from the $|d^6(A_1).s(E'); E':1e\rangle$ and $|d^6(T_1).s(E'); E':1e\rangle$ (one-phonon) and the $|d^6(E).s(E'); U'\rangle$ (no-phonon) states, all of which split as doublets. The smaller splitting into four components derives from admixture of other U′ states with fourfold Zeeman patterns.

The magnitudes of the parameters used to fit the Zeeman data in figure 10 and the absorption spectrum in figure 1 are as follows:

$$\left.\begin{aligned} \gamma &= 1 \equiv 56\,\mathrm{cm}^{-1}, \\ \hbar\omega_E &= 0.5 \equiv 28\,\mathrm{cm}^{-1}, \\ D &= 0.55 \equiv 30\,\mathrm{cm}^{-1}, \\ V/\alpha &= 0.6 \equiv 33.6\,\mathrm{cm}^{-1}, \end{aligned}\right\} \tag{43}$$

where α is a characteristic of the J–T active mode (see Appendix). The value of V/α adopted here is equivalent to a J–T energy $E_{JT} = V^2/2\alpha^2\hbar\omega_E = 20.2\,\mathrm{cm}^{-1}$. This is clearly within the dynamic J–T régime. However, the fact that E_{JT} is comparable with the value of $\hbar\omega_E$ above suggests that the restriction to two-phonon states (§ 5 (*d*)) is inadequate. Our approach to the J–T problem must therefore be regarded as illustrative rather than quantitative. The energy *D* is equivalent to a splitting of the ^4E and ^6E states induced by the exchange interaction of $\frac{5}{3}D \approx 51\,\mathrm{cm}^{-1}$, less than one quarter of the overall second-order spin–orbit splitting $4\gamma = 224\,\mathrm{cm}^{-1}$.

TABLE 1. SPIN–ORBIT AND JAHN–TELLER ENERGY PARAMETERS (cm^{-1}) FOR THE $d^6(^5E)$ CONFIGURATION

	γ	$\hbar\omega_E$	V/α	reference
$ZnS:Fe^{2+}$	15.0	—	—	Ham & Slack (1971)
$GaP:Fe^{2+}$	14.7	25.2	0.35	West *et al.* (1980)
$CdTe:Fe^{2+}$	20.8	38	17.9	Vallin (1970)
$[ZnSe:Co^{3+}]$	56	28	33.6	this work

Since the spin–orbit and J–T interactions are assumed to occur within the $[Co^{3+}(d^6, {}^5E)]$ core of the excited state it is of interest to compare the relevant parameters used here with those found for the divalent $Fe^{2+}(d^6, {}^5E)$ impurity in zinc-blende materials. This comparison is made in

table 1. The value of the spin–orbit parameter γ for $[Co^{3+}(d^6, {}^5E)]$ is some 2.7–3.8 times the values quoted for Fe^{2+}. However,

$$\gamma \sim 6(\lambda^2/\Delta), \tag{44}$$

where λ is the effective spin–orbit coupling constant for the impurity, and Δ the T_d ligand field energy (Ham & Slack, 1971). To a first approximation, the parameter γ therefore increases as the square of the spin–orbit coupling energy. The magnitude of γ derived from the model implies an increase in spin–orbit coupling energy λ by a factor of *ca.* 1.6 to 2.0 for the $[Co^{3+}(d^6, {}^5E)]$ system, compared with $Fe^{2+}(d^6, {}^5E)$. This is not unreasonable in view of the fact that both the atomic number and the formal oxidation state increase on going from Fe^{2+} to Co^{3+}. The J–T parameter V/α is also significantly larger for the $[Co^{3+}(d^6, {}^5E)]$ system. This may again be related to the higher formal charge state of the impurity, generating an increase in the coupling strength.

It is normally assumed that the J–T active vibrational mode of e symmetry involves motion of the four nearest-neighbour anions surrounding the impurity. The lowest energy peak in the ZnS zinc-blende phonon density-of-states which projects out a mode of e symmetry at the impurity site is that of the TA(L) phonons (Ham & Slack 1971). This peak occurs at *ca.* 58 cm^{-1} in ZnSe (Radlinski 1978). Although the energy of the J–T active mode in the model, $\hbar\omega_E = 28\,cm^{-1}$, is comparable with values used in treating $Fe^{2+}(d^6, {}^5E)$ (see table 1), it is appreciably smaller than the TA(L) phonon energy. However, the limitations of our theory (see above) do not make it possible to give a precise interpretation of $\hbar\omega_E$.

One final point of interest is the insight that the model gives into the anisotropic stress splittings of the low energy lines, summarized in figure 4. The L line involves a Kramers doublet excited state of E′ symmetry. Therefore, with a small unresolved splitting of the $^4A_2(F)$ ground state this will remain a single line for any stress direction. The L′ line, with excited state of U′ symmetry, splits into two resolved components for $P \parallel [111]$, but is unsplit for $P \parallel [001]$. As noted in discussing the unusual Zeeman splitting of the L′ line, the dominant contributions to the excited state wavefunction come from the $|d^6(A_1).s(E'); E': 1e\rangle$, $|d^6(T_1).s(E'); E': 1e\rangle$ and $|d^6(E).s(E'); U'\rangle$ states, the latter being mixed by the J–T interaction. The $[Co^{3+}(d^6, {}^5E)]$ core has the electronic configuration $[e^3t_2^3]$, with one hole in the e orbitals derived from the free-ion d-orbitals which determines the overall E orbital symmetry of the $d^6(^5E)$ state.

In the unperturbed cubic (T_d) point group, the e orbitals have zero orbital moment. With quantization along the [001] direction these orbitals transform as $e_\theta = (d_0)$ and $e_\epsilon = \frac{1}{\sqrt{2}}d_2 + \frac{1}{\sqrt{2}}d_{-2}$ (Ballhausen 1962). For tetragonal stress $P \parallel [001]$ these orbitals undergo equal and and opposite splittings, and the twofold E-orbital degeneracy is lifted. However, the combination of spin–orbit and spin–spin interactions effectively stabilizes the major components of the L′ excited-state wavefunction against any splitting under tetragonal stress. The $|d^6(A_1).s(E'); E': 1e\rangle$ state can show no first-order electron–phonon interactions. The other *electronic* basis states can be expanded to give (Griffith 1964):

$$\begin{aligned}|d^6(T_1).s(E'); E'\alpha'\rangle &= \tfrac{1}{\sqrt{3}}\,|d^6(^5E)\,T_1\,0\rangle\,|s(^2A_1).E'\alpha'\rangle - \sqrt{\tfrac{2}{3}}\,|d^6(^5E)\,T_1\,1\rangle\,|s(^2A_1)\,E'\beta'\rangle \\ &= \tfrac{1}{\sqrt{6}}[|^5E: 2\varepsilon\rangle - |^5E: -2\varepsilon\rangle]\,|^2A_1: E'\alpha'\rangle \\ &\quad + [\tfrac{1}{\sqrt{2}}\,|^5E: 1\theta\rangle + \tfrac{1}{\sqrt{6}}\,|^5E: -1\varepsilon\rangle]\,|^2A_1: E'\beta'\rangle, \end{aligned} \tag{45}$$

$$\begin{aligned}|d^6(E).s(E'); U'_\kappa\rangle &= |d^6(^5E)\,E\varepsilon\rangle\,|s(^2A_1)\,E'\beta'\rangle \\ &= [\tfrac{1}{2}\,|^5E: 2\theta\rangle + \tfrac{1}{2}\,|^5E: -2\theta\rangle + \tfrac{1}{\sqrt{2}}\,|^5E: 0\varepsilon\rangle]\,|^2A_1: E'\beta'\rangle, \end{aligned} \tag{46}$$

where $|^5E: M_S M_L\rangle$ and $|^2A_1: E'\alpha'(\beta')\rangle$ are states of the residual impurity core and the bound electron respectively. The spin–spin coupling in equation (45) ensures that the $M_L = \theta$ and $M_L = \varepsilon$ orbital components are equally weighted in the electronic basis functions, a necessary condition to prevent stress-induced splitting of the Kramers doublet $|d^6(T_1).s(E'); E'\rangle$ state. The second-order spin–orbit coupling in equation (46) ensures the same equal weighting, so that the $|d^6(E).s(E'); U'\rangle$ zero-phonon state is also unsplit for $P \| [001]$. This stabilization of the $|d^6(^5E)\, E\rangle$ spin–orbit component against tetragonal stress is evident in the small parameter $B_3 = 0.002\,\mathrm{cm}^{-1}$ $(\mathrm{N\,mm}^{-2})^{-1}$ for the $E(\Gamma_3)$ spin–orbit state of $Fe^{2+}(d^6, {}^5E)$ in GaP (West *et al.* 1980). Stress applied parallel to [001] therefore induces no first-order splittings or changes in interaction strength involving the basis states dominating the L′ excited-state wavefunction, and this line remains unsplit.

The situation is rather different for $P \| [111]$, however, where the $M_L = \theta$, ε orbital components remain degenerate in the reduced C_{3V} point-group symmetry of the perturbed impurity. For the unperturbed impurity, with quantization along the [111] direction, the e orbitals transform in T_d as $\frac{1}{\sqrt{3}}d_2 + \sqrt{\frac{2}{3}}d_{-1}$ and $\frac{1}{\sqrt{3}}d_{-2} - \sqrt{\frac{2}{3}}d_1$ (Ballhausen 1962). This ratio of coefficients, which ensures a zero orbital moment, is determined by the fourfold rotational symmetry in the T_d point group. This fourfold symmetry axis is removed under trigonal stress, and the relative coefficients for the $d_{\pm 2}$ and $d_{\mp 1}$ orbitals can change. That is, the trigonal stress distorts the e orbitals and induces a non-zero orbital moment by mixing with the t_2 orbitals. The $|d^6(^5E)\, T_1\rangle$ and $|d^6(^5E)\, E\rangle$ spin–orbit states include components of this induced orbital moment. The spin of the bound electron e_b in the c.t. state is then able to couple to this orbital angular momentum via some combination of the various spin–orbital interactions represented by the term $\mathscr{H}_{EX}$ in the Hamiltonian. The effect of trigonal distortion is therefore to change the nature of the coupling within the c.t. excited state, giving a spin–orbit interaction energy proportional to the applied trigonal stress. This spin–orbit energy can split the basis states contributing to the L′ excited state wavefunction. For example, in the C_{3V} point group the $|d^6(^5E)\, E\rangle$ core state transforms as Γ_3, and the bound electron e_b as Γ_4 (Koster *et al.* 1963). The direct product gives:

$$[\Gamma_3 \times \Gamma_4] = \Gamma_4 + (\Gamma_5, \Gamma_6), \tag{47}$$

with Γ_4 transforming as $M_J = \pm\frac{1}{2}$ and (Γ_5, Γ_6) as $M_J = \pm\frac{3}{2}$. These Γ_4 and (Γ_5, Γ_6) states will be split by the stress-induced spin–orbit coupling energy. The Γ_4 component of the perturbed L′ excited state presumably moves to low energy, eventually interacting with the Γ_4 state derived from the $E'(T_d)$ excited state of the L origin line. This is the probable source of the nonlinear effects for $P \| [111]$ discussed in § 3.3.

6. Conclusions

Qualitative arguments have been presented in § 4 to suggest that the three near-gap absorption bands in ZnSe:Co, illustrated in figures 3*a–c*, can only be assigned consistently as impurity → c.b. c.t. transitions of the kind represented in equation (1). A more quantitative model for the c.t. excited state has been developed in § 5, and shown to give excellent quantitative agreement with the Zeeman splitting and polarization data for the lowest energy band. Additionally, the model offers an explanation for features in the absorption spectrum not associated with the lattice phonon density-of-states, and for the highly anisotropic stress splitting of the L′ line at

2.363 eV. The evidence is therefore strong that the L band in ZnSe:Co with origin at 2.361 eV arises from a c.t. excitation of the kind

$$Co^{2+}_{Zn}(d^7) \rightarrow [Co^{3+}(d^6, {}^5E)] \,.\, e_b. \tag{48}$$

To the best of our knowledge this represents the first report of a transition of this kind.

The physics of the model for the c.t. excited state are easily appreciated. It consists of two relatively weakly coupled parts, with the lowest energy state having the residual $[Co^{3+}(d^6)]$ core in the ^5E ligand field state, analogously to the well known example $Fe^{2+}(d^6, {}^5E)$. The perturbations represented by essentially one-electron operators, i.e. the spin–orbit and the J–T coupling, are dominated by interactions within the tightly bound residual $[Co^{3+}(d^6, {}^5E)]$ core. The excited electron e_b is bound by some combination of coulombic and central-cell forces. A weak spin-dependent interaction between the bound electron and the residual core electrons is introduced in the form of a very simplified spin–spin exchange interaction. With the assumptions discussed in the text, the model involves four disposable parameters plus a constant electron binding energy. Although too much significance should not be attached to the values of these parameters in a model of this kind, especially to the spin-dependent exchange coupling energy D, the magnitudes of the spin–orbit and J–T parameters (γ and V/α) used to fit the L band are quite reasonable compared with those for the analogous $Fe^{2+}(d^6, {}^5E)$ impurity. The energy of the J–T active mode, $\hbar\omega_E = 28\,\mathrm{cm}^{-1}$, is however significantly less than the TA(L) peak in the phonon density of states, this being the lowest energy lattice-phonon peak that projects a mode of e symmetry at the impurity site (see § 5 (*e*)).

Within our model, the higher energy absorption bands, M and N, are to be assigned as transitions to higher energy excited states of the c.t. configuration $[Co^{3+}(d^6)] \,.\, e_b$. These higher energy charge transfer configurations could in principle arise from either higher-energy ligand field states of the $[Co^{3+}(d^6)]$ core, or from less tightly bound states of the excited electron. The first of these possibilities is unlikely, since the total energy separation between L and N (*ca.* 185 meV) is much smaller than any reasonable ligand field energy Δ. It is probable that the $^5T_2(d^6)$ state remains the lowest energy excited ligand field state of $[Co^{3+}, d^6]$; for $Fe^{2+}(d^6)$ in ZnSe, the lowest energy spin–orbit component of $^5T_2$ is *ca.* 339 meV above ^5E (Baranowski *et al.* 1967), and a larger separation is expected for the $[Co^{3+}(d^6)]$ system. We are therefore led to suggest that the M and N transitions involve excited states in which the excited electron is less tightly bound. The general excitation process is then:

$$[Co^{2+}_{Zn}(d^7)] \rightarrow [Co^{3+}_{Zn}(d^6, {}^5E)] \,.\, e^{\alpha}_b \quad (\alpha = L, M, N). \tag{49}$$

The $Co^{2+}_{Zn}(d^7)$ ground state in figure 12*a* has been placed *ca.* 2.55 eV below the c.b., on the assumption that the onset of the continuum in the $^4T_2(F) \rightarrow {}^4A_2(F)$ p.l.e. spectrum of $Co^{2+}_{Zn}(d^7)$ (I, figure 2) represents the threshold for ionization of the excited electron. A strong threshold near this energy is also observed in photocapacitance (Noras *et al.* 1980). The excited-state binding energies on this model are *ca.* 189 meV (e^L_b), *ca.* 118 meV (e^M_b) and *ca.* 4 meV (e^N_b), to be compared with an effective mass donor binding energy $E_D^{e.m.} \approx 26$ meV in ZnSe (Dean *et al.* 1981 *b*). The value for e^N_b is of course approximate because of uncertainty in the threshold. However, it would appear that only in this highest energy state is the electron binding likely to be at all effective-mass-like, and probably represents transitions to the $n = 2$ orbital excited state of the electron bound to the charged $[Co^{3+}_{Zn}(d^6)]$ core. This state is expected to have a binding energy of *ca.* 6.5 meV, or slightly less if we allow for the effect of the extended charge of the $[Co^{3+}_{Zn}(d^6)]$ core on the electron binding energy in the hydrogenic model. Actually, the relatively broad line N is

likely to contain an unresolved average of contributions from a series of such coulombic excited states with $n \geqslant 2$, which will further reduce the binding energy apparent from its centre of gravity. Line M, which represents transitions to a state of binding energy *ca.* 120 meV, $\gg E_D^{e.m.}$, must represent a second excited state whose binding energy is essentially determined by the short-range part of the $[Co_{Zn}^{3+}(d^6)]$ potential, like that for L. It is therefore perhaps not surprising that the three lines L, M and N do not follow a simple Rydberg sequence. As the binding energy decreases, the orbital radius of the excited electron will increase, but it is misleading to describe the orbits of the relatively deeply bound electron states for L and M in purely hydrogenic terms, i.e. 1s, 2s, ..., etc. (Jaros 1980). However, the relative magnitudes of the various interactions within the c.t. state are likely to change as the effective radius of the bound electron increases, producing some changes in line-shape and splittings under stress and magnetic field perturbations.

The observation of luminescence from the lowest-energy c.t. state of Co_{Zn} after above-gap excitation, and particularly for excitation energies close to $E_{g.x.}$ as with a He–Cd laser, is particularly significant in giving insight into the mechanism of energy relaxation involving metal ion impurities in semiconductors and phosphors (Robbins & Dean 1978). As noted in § 4 (*b*), this c.t. state can be considered a form of deep bound exciton (b.e.) state which can be created by sequential capture of a hole and electron:

$$\text{(i)} \qquad h\nu \rightarrow e_c + h_v, \tag{50}$$

$$\text{(ii)} \qquad [Co_{Zn}(d^7)]^0 + h_v \rightarrow [Co_{Zn}(d^6)]^+, \tag{51}$$

$$\text{(iii)} \qquad [Co_{Zn}(d^6)]^+ + e_c \rightarrow [Co_{Zn}(d^6)]^+ . e_b, \tag{52}$$

where the superscripts indicate effective charge with respect to the lattice. Since the $[Co_{Zn}(d^7)]$ level lies less than about 300 meV above the v.b., the hole-capture rate should be fast. The fact that the 2.361 eV c.t. state luminescence is excited relatively strongly by ionizing radiation (e.g. in cathodoluminescence) shows that relaxation of free electrons and holes through this c.t. state is an efficient process, as suggested by Robbins & Dean (1978). A second example which has been recently studied, and which further illustrates this point, is the radiative v.b. → impurity c.t. transition of ZnO:Cu (Dingle 1969; Dean *et al.* 1981 *a*; Robbins *et al.* 1981). Luminescence from this c.t. state is also excited efficiently by ionizing radiation. However, in this case it is presumably the electron that is bound first in the relaxation sequence:

$$\text{(i)} \qquad h\nu \rightarrow e_c + h_v, \tag{53}$$

$$\text{(ii)} \qquad [Cu(d^9)]^0 + e_c \rightarrow [Cu(d^{10})]^-, \tag{54}$$

$$\text{(iii)} \qquad [Cu(d^{10})]^- + h_v \rightarrow [Cu(d^{10})]^- . h_b. \tag{55}$$

Finally, the significance of transitions of this kind in understanding the electronic states of TM impurities in solids should be emphasized. First, their observation gives a good estimate of the position of the impurity ground state with respect to the band edges. The fine structure associated with particular absorption and luminescence bands may unambiguously connect an ionization transition with a given impurity charge state, as for the impurity → c.b. c.t. transition of Co_{Zn}. If further examples can be identified, this will help greatly in understanding the factors controlling the level energies for different TM impurities. It is worth noting here that rather similar absorption bands to those analysed for ZnSe:Co are also observed in ZnS:Co (Noras *et al.* 1980).

Secondly, the excited states in the impurity → c.b. c.t. transition (equation (12)) and in the

v.b. → impurity c.t. transition (equation (11)) have configurations analogous to deep donors and acceptors, respectively. The excited particle in the lowest energy state is bound largely by short-range central cell forces; the fine structure in the optical spectra and the observation of higher excited states should be rich sources of information on the detailed interactions between the bound particle and the impurity core. The fine structure observed in the optical spectra of ZnSe:Co and ZnO:Cu points to the potential importance of both these systems in the general theoretical study of deep levels in solids.

The authors are grateful to Dr J. M. Noras, Dr J. W. Allen and Dr H. R. Szawelska for providing results before publication, and for permission to reproduce the absorption spectrum in figure 1 *a*. They also wish to thank Dr M. S. Skolnick for measurement of the circularly polarized spectra in figure 9, Mr J. L. Glasper for assistance in the luminescence measurements and Dr D. C. Herbert for many helpful discussions on theoretical aspects of this work.

References

Allen, J. W. 1980 Private communication.
Ballhausen, C. J. 1962 *Introduction to ligand field theory*. New York: McGraw Hill.
Baranowski, J. M., Allen, J. W. & Pearson, G. L. 1967 *Phys. Rev.* **160**, 627.
Bishop, S. G., Robbins, D. J. & Dean, P. J. 1980 *Solid St. Commun.* **33**, 119.
Dean, P. J. & Herbert, D. C. 1979 Bound excitons. In *Excitons* (ed. K. Cho), *Topics in current physics*, vol. 14, p. 55. Berlin: Springer-Verlag.
Dean, P. J., Robbins, D. J., Bishop, S. G., Savage, J. A. & Porteous, P. 1981*a* *J. Phys.* C **14**, 2847.
Dean, P. J., Bhargava, R. N., Fitzpatrick, B. J., Herbert, D. C. & Werkhoven, C. J. 1981*b* *Phys. Rev.* B **23**, 4888.
Dingle, R. 1969 *Phys. Rev. Lett.* **23**, 579.
Fano, U. 1961 *Phys. Rev.* **124**, 1866.
Fano, U. & Cooper, J. W. 1968 *Rev. mod. Phys.* **40**, 441.
Griffith, J. S. 1962 *The irreducible tensor method for molecular symmetry groups*. Englewood Cliffs, New Jersey: Prentice-Hall.
Griffith, J. S. 1964 *The theory of transition metal ions*. Cambridge University Press.
Ham, F. S., Ludwig, G. W., Watkins, G. D. & Woodbury, H. H. 1960 *Phys. Rev. Lett.* **5**, 468.
Ham, F. S. & Slack, G. A. 1971 *Phys. Rev.* B **4**, 777.
Hennel, A. M. & Uba, S. M. 1978 *J. Phys.* C **11**, 4565.
Jaros, M. 1980 *Adv. Phys.* **29**, 409.
Judd, B. R. 1963 *Operator techniques in atomic spectroscopy*. New York: McGraw Hill.
Kaplyanskii, A. A. 1964 *Optics Spectrosc.* **16**, 557.
Kosai, K., Fitzpatrick, B. J., Grimmeiss, H. G., Bhargava, R. N. & Newmark, G. F. 1979 *Appl. Phys. Lett.* **35**, 194.
Koster, G. F., Dimmock, J. O., Wheeler, R. G. & Statz, H. 1963 *Properties of the thirty-two point groups*. Cambridge, Massachusetts: MIT Press.
Kunc, K., Balkanski, M. & Nusimovici, M. A. 1975 *Physica Status Solidi* b **72**, 229.
McClure, D. S. 1959 *Electronic spectra of molecules and ions in crystals*. New York: Academic Press.
Noras, J. M. & Allen, J. W. 1980 *J. Phys.* C **13**, 3511.
Noras, J. M., Szawelska, H. R. & Allen, J. W. 1980 Private communication.
Radlinski, A. P. 1977 *Physica Status Solidi* b **84**, 503.
Radlinski, A. P. 1978 *Physica Status Solidi* b **86**, 41.
Radlinski, A. P. 1979 *J. Lumin.* **18/19**, 147.
Robbins, D. J. & Dean, P. J. 1978 *Adv. Phys.* **27**, 499.
Robbins, D. J., Dean, P. J., Glasper, J. L. & Bishop, S. G. 1980 *Solid St. Commun.* **36**, 61. (Paper I.)
Robbins, D. J., Herbert, D. C. & Dean, P. J. 1981 *J. Phys.* C **14**, 2859.
Uba, S. M. & Baranowski, J. M. 1978 *Phys. Rev.* B **17**, 69.
Vallin, J. T. 1970 *Phys. Rev.* B **2**, 2390.
Vogel, E. E. & Rivera-Iratchet, J. 1980 *Phys. Rev.* B **22**, 4511.
Weakliem, H. A. 1962 *J. chem. Phys.* **36**, 2117.
Weber, J., Ennen, H., Kaufman, U. & Schneider, J. 1980 *Phys. Rev.* B **21**, 2394.
West, C. L. 1980 D.Phil. thesis, Oxford University.
West, C. L., Hayes, W., Ryan, J. F. & Dean, P. J. 1980 *J. Phys.* C **13**, 5631.
Wray, E. M. & Allen, J. W. 1971 *J. Phys.* C **4**, 512.

PHILOSOPHICAL TRANSACTIONS OF THE ROYAL SOCIETY A MATHEMATICAL, PHYSICAL & ENGINEERING SCIENCES

PHILOSOPHICAL TRANSACTIONS OF THE ROYAL SOCIETY A MATHEMATICAL, PHYSICAL & ENGINEERING SCIENCES

TABLE 2. MATRIX OF THE SYSTEM HAMILTONIAN (A 1)

$\Gamma'\gamma' = E'\alpha'$	$\lvert A_1.E'\rangle_0$	$\lvert T_1.E'\rangle_0$	$\lvert E.E'\rangle_{1e}$	$\lvert T_1.E'\rangle_{1e}$	$\lvert T_2.E'\rangle_{1e}$	$\lvert A_1.E'\rangle_{2a_1}$	$\lvert T_1.E'\rangle_{2a_1}$	$\lvert E.E'\rangle_{2e}$	$\lvert T_1.E'\rangle_{2e}$	$\lvert T_2.E'\rangle_{2e}$
	$+\beta H$	$\frac{2}{\sqrt{6}}D+1.63\beta H$	$-V/\alpha$	0	0	0	0	0	0	0
		$\gamma-\frac{1}{3}D+\frac{1}{3}\beta H$	0	$\frac{1}{\sqrt{2}}V/\alpha$	$\frac{1}{\sqrt{2}}V/\alpha$	0	0	0	0	0
			$2\gamma+\hbar\omega_E+\beta H$	$-\frac{2\sqrt{3}}{6}D-1.16\beta H$	$\frac{2\sqrt{3}}{6}D+1.16\beta H$	$-V/\alpha$	0	0	0	0
				$(\gamma+\hbar\omega_E+\frac{1}{6}D-0.67\beta H)$	$\frac{1}{2}D-\beta H$	0	$\frac{1}{\sqrt{2}}V/\alpha$	0	$-\frac{1}{\sqrt{2}}V/\alpha$	$-\frac{1}{\sqrt{2}}V/\alpha$
					$(3\gamma+\hbar\omega_E+\frac{1}{6}D-0.67\beta H)$	0	$-\frac{1}{\sqrt{2}}V/\alpha$	0	$-\frac{1}{\sqrt{2}}V/\alpha$	$-\frac{1}{\sqrt{2}}V/\alpha$
						$2\hbar\omega_E+\beta H$	$\frac{2}{\sqrt{6}}D+1.63\beta H$	0	0	0
							$(\gamma+2\hbar\omega_E-\frac{1}{3}D+\frac{1}{3}\beta H)$	0	0	0
								$(2\gamma+2\hbar\omega_E+\beta H)$	$-\frac{2\sqrt{3}}{6}D-1.16\beta H$	$\frac{2\sqrt{3}}{6}D+1.16\beta H$
									$(\gamma+2\hbar\omega_E+\frac{1}{6}D-0.67\beta H)$	$\frac{1}{2}D-\beta H$
										$(3\gamma+2\hbar\omega_E+\frac{1}{6}D-0.67\beta H)$

Appendix. The matrix of the system Hamiltonian

The matrix of the system Hamiltonian

$$\mathscr{H} = \mathscr{H}_{SO} + \mathscr{H}_{EX} + \mathscr{H}_{JT} + \mathscr{H}_{Z} \tag{A 1}$$

is given in table 2 for the vibronic basis set of E′ symmetry, a single J–T active mode of energy $\hbar\omega_E$ being assumed. The constant term $\mathscr{H}_0$ is neglected. The basis is truncated at the two-phonon states. The kets are the electronic product states defined in equations (17)–(23), but the notation is abbreviated to show only the spin–orbit components of the [$Co^{3+}(d^6, {}^5E)$] core and of the bound electron, E′. The phonon occupancy is indicated by the subscript, for example, $|\rangle_{2e}$ indicates a vibrational state of e symmetry derived from a two-phonon occupancy. The constant α appears from the matrix elements of the harmonic oscillator wavefunctions, and is characteristic of the vibrational mode (Vallin 1970)

$$\alpha = (\mu\omega_E/\hbar)^{\frac{1}{2}}, \tag{A 2}$$

β is the Bohr magnetron, and the other parameters are defined in the text. The matrix is Hermitian.